

**NASA CONTRACTOR
REPORT**



NASA-CR-814

C.1

0060693



TECH LIBRARY KAFB, NM

NASA CR-1424

LOAN COPY: RETURN TO
AFWL (WLIL-2)
KIRTLAND AFB, N MEX

**STRUCTURAL OPTIMIZATION OF
SANDWICH AND RING-STIFFENED
120 DEGREE CONICAL SHELLS
SUBJECTED TO EXTERNAL PRESSURE**

by Gerald A. Cohen

Prepared by

PHILCO-FORD CORPORATION

Newport Beach, Calif.

for Langley Research Center

NATIONAL AERONAUTICS AND SPACE ADMINISTRATION • WASHINGTON, D. C. • AUGUST 1969



0060693

NASA CR-1424

STRUCTURAL OPTIMIZATION OF SANDWICH
AND RING-STIFFENED 120 DEGREE CONICAL SHELLS
SUBJECTED TO EXTERNAL PRESSURE

By Gerald A. Cohen

Distribution of this report is provided in the interest of information exchange. Responsibility for the contents resides in the author or organization that prepared it.

Prepared under Contract No. NAS 1-5554-6 by
PHILCO-FORD CORPORATION
Space and Re-entry Systems Division
Newport Beach, Calif.

for Langley Research Center

NATIONAL AERONAUTICS AND SPACE ADMINISTRATION

PREFACE

This study was initiated while the author was employed by the Philco-Ford Corporation. Technical responsibility for the completion of the work and the preparation of this report resides in Structures Research Associates under subcontract to Philco-Ford. The contribution of Charles G. Dietz, who assisted in the analysis, is gratefully acknowledged.

ABSTRACT

A practical optimum design procedure is developed for lightly loaded shells of revolution of both sandwich and ring-stiffened construction. For ring-stiffened shells, this procedure employs a design computer program as well as shell prebuckling and buckling analysis programs. Specific point designs for 120° truncated cones are obtained over a wide range of critical pressure for two base radii. The results show that for low loading, ring-stiffened construction is more efficient than sandwich construction.

CONTENTS

	Page
SUMMARY	1
INTRODUCTION	2
SYMBOLS	3
DESIGN SPECIFICATIONS	6
Geometry, Loading, and Material Considerations	6
Shell Wall Construction	7
Honeycomb sandwich wall	7
Ring-stiffened wall	7
Range of Parameters	7
METHOD OF STRUCTURAL SYNTHESIS	7
Design-Analysis Iteration Procedure	7
Base Ring Design	8
Nose Ring Design	9
Sandwich shell nose ring	9
Ring-stiffened shell nose ring	9
Shell Design	10
Sandwich cones	10
Ring-stiffened shells	11
Shell Analysis	18
RESULTS	19
Sandwich Cones	19
Ring-Stiffened Cones	20
Configuration Comparison	23
CONCLUDING REMARKS	25
APPENDIX A - DETERMINATION OF STRESS RESULTANTS OF RING-STIFFENED SHELLS USING MEMBRANE THEORY	26
APPENDIX B - SANDWICH CONE CORRELATIONS	28
Base ring	28
Sandwich shell	29
REFERENCES	30
TABLES	32
FIGURES	39

STRUCTURAL OPTIMIZATION OF SANDWICH AND
RING-STIFFENED 120 DEGREE CONICAL SHELLS
SUBJECTED TO EXTERNAL PRESSURE

by

Gerald A. Cohen

Structures Research Associates, Newport Beach, California

SUMMARY

Optimum design procedures are developed for lightly loaded, blunt truncated shells of revolution of both sandwich and ring-stiffened construction. The procedures developed consist of an iteration between design, based on certain approximations, and analysis, evaluating and modifying these approximations. The analysis is performed by existing shell prebuckling and buckling computer programs. The design step for ring-stiffened shells necessitated the development of a new computer program. This program allows variable ring size and spacing distributions, and trades off ring weight with shell skin weight to achieve minimum total weight. The optimization is performed subject to the constraints necessary to insure fabrication feasibility.

Using this iteration procedure, optimum point designs have been obtained for sandwich and ring-stiffened 120° truncated conical shells at three nominal ratios of critical pressure to Young's modulus, viz. $p/E = 2, 10, \text{ and } 50 \times 10^{-7}$. In order to assess the effect of minimum gage constraints, designs have been obtained for two values of the base radius, 57 in. and 114 in. Least square algebraic correlations have been fitted to the sandwich cone results, thus making possible interpolation between, and extrapolation beyond the point designs obtained.

Results are presented in the form of curves of dimensionless weight versus dimensionless critical pressure for each value of the base radius. The main conclusion to be drawn from these results is that at low loading ring-stiffened construction is structurally superior, whereas at relatively high loading sandwich construction is structurally superior. This crossover is caused primarily by minimum gage constraints, which impose, at low

STRUCTURAL OPTIMIZATION OF SANDWICH AND
RING-STIFFENED 120 DEGREE CONICAL SHELLS

SUBJECTED TO EXTERNAL PRESSURE

by

Gerald A. Cohen

Structures Research Associates, Newport Beach, California

SUMMARY

Optimum design procedures are developed for lightly loaded, blunt truncated shells of revolution of both sandwich and ring-stiffened construction. The procedures developed consist of an iteration between design, based on certain approximations, and analysis, evaluating and modifying these approximations. The analysis is performed by existing shell prebuckling and buckling computer programs. The design step for ring-stiffened shells necessitated the development of a new computer program. This program allows variable ring size and spacing distributions, and trades off ring weight with shell skin weight to achieve minimum total weight. The optimization is performed subject to the constraints necessary to insure fabrication feasibility.

Using this iteration procedure, optimum point designs have been obtained for sandwich and ring-stiffened 120° truncated conical shells at three nominal ratios of critical pressure to Young's modulus, viz. $p/E = 2, 10, \text{ and } 50 \times 10^{-7}$. In order to assess the effect of minimum gage constraints, designs have been obtained for two values of the base radius, 57 in. and 114 in. Least square algebraic correlations have been fitted to the sandwich cone results, thus making possible interpolation between, and extrapolation beyond the point designs obtained.

Results are presented in the form of curves of dimensionless weight versus dimensionless critical pressure for each value of the base radius. The main conclusion to be drawn from these results is that at low loading ring-stiffened construction is structurally superior, whereas at relatively high loading sandwich construction is structurally superior. This crossover is caused primarily by minimum gage constraints, which impose, at low

loading, a greater limitation on sandwich construction than on ring-stiffened construction. As an example, for aluminum construction the crossover pressures are 8.9 and 18.9 psi for the 114 and 57 inch base radii, respectively.

INTRODUCTION

Reference 1 presents the results of an analysis of the buckling strength of two 120° truncated conical shells differing in wall construction, one being of sandwich construction and the other of ring stiffened construction. The shells were designed for equal weight and had dimensions typical of a planetary entry capsule. The results indicated that the sandwich wall can withstand roughly 50% more pressure, although requiring a somewhat heavier base ring to achieve this superiority. The two designs considered, however, are nonoptimum, and it is therefore desirable to re-evaluate these two important types of construction when both are structurally optimized.

Previous attempts at optimum design of stiffened conical shells are presented in References 2 and 3. Both of these studies were based on hydrostatic pressure loading and treated primarily rectangular interior rings of constant cross section. Neither the necessary edge support nor the constraints imposed by manufacturing limitations were considered. The essential difference between these two studies is that in Reference 2 only equally spaced rings were considered, whereas in Reference 3 prechosen variable spacing laws were considered.

In this paper practical optimum design procedures for lightly loaded sandwich and ring-stiffened cones are developed. The design of the ring-stiffened cones required the development of a design computer program, which incorporates and extends some of the basic ideas of References 2 and 3. In the development of this program, sufficient generality was retained so that it may be used for more general shells of revolution. These methods were applied in References 4 and 5 to specific point designs of Mars entry capsules of various geometrical shapes, including 120° cones, for one size and aerodynamic pressure distribution. In this paper the ranges of loading and size chosen include the probable ranges of these parameters to be encountered by practical Mars entry capsules.

SYMBOLS

A	ring section area, in. ² ; or stringer section area, in. ²
C	general instability correlation factor
D	shell flexural rigidity, lb-in.
d	local value of interior ring spacing, in.
d _r	rivet diameter, in.
E	Young's modulus, psi
e	eccentricity of centroid of ring-shell composite wall from the middle surface of shell skin, in.
f _R	riveted flange width, in.
h	thickness of Z-section interior ring, in.
h ₁	value of h defined in Figure 3, in.
I	ring section moment of inertia, in. ⁴
I _e	interior ring section moment of inertia about centroid of composite wall, in. ⁴
k	maximum value of η ; or compressive stress coefficient
L	meridional length of truncated shell, in.
ℓ	ideal cross section perimeter of Z-section interior ring, in.
ℓ_1	value of ℓ defined in Figure 3, in.
M	number of interior rings

N	circumferential harmonic number
n	number of stringers
P	axial load, lb
p	(critical) pressure, psi
R	radius of curvature, in.
r	radial distance from axis of revolution, in.
s	meridional distance from small edge of shell
T	(critical) shell stress resultant, lb/in.
T_ϕ	(critical) ring stress resultant, lb
t	shell or edge ring thickness, in.
\tilde{t}	minimum of t and h, in.
W	structural weight, lb
w	normal deflection of buckling mode, in.
x, y	axial and radial coordinates, respectively; or sandwich shell correlation parameters; or interior ring and stringer parameters
z	geometrical factor for axial force equilibrium, in.
α	cone half-angle, deg
γ, κ	sandwich shell instability correlation constants

Δ	increase in riveted flange width of interior ring necessary to accommodate a rivet, in.
ΔT_1	increment in meridional stress resultant due to stringers, lb/in.
ϵ	strain
η	relative increase in hoop flexural rigidity due to ring stiffening
λ	load factor
μ	surface density of sandwich cone adhesive, lb/ft ²
ν	Poisson's ratio
ρ	density, lb/in. ³
σ	(critical) stress, psi
τ	$\rho_c/2\rho_f$

Subscripts:

a	value at small end of shell
b	value at large end of shell
c	pertaining to sandwich core; or critical value
cyl	pertaining to the cylindrical element of sandwich shell nose rings
d	design value

f	pertaining to sandwich face sheet
f1	pertaining to the radial flange of sandwich shell nose rings
min	minimum gage
o	critical value for pure hydrostatic or axial loading
R	pertaining to an interior ring
S	pertaining to a stringer
wash	pertaining to the washer plate element of ring-stiffened shell nose rings
1	meridional component
2	circumferential component
Superscripts:	
($\bar{}$)	average value

DESIGN SPECIFICATIONS

The structural designs obtained are subject to several design specifications, which, in effect, define the problem treated.

Geometry, Loading, and Material Considerations

The basic configuration considered is a 120° full angle conical shell truncated at a radius equal to $1/3$ of the base radius, and loaded by a uniform external pressure applied to its lateral surface (Figure 1). The axial resultant of this loading is reacted by a circular line load ($\approx 4pr_b/3$) applied at the centroidal axis of an attachment (nose) ring supporting the small edge of the shell. There is also a tubular base ring, supporting the large edge of the shell, which is free of external load. Both nose and base rings are attached internally to the shell. Each design is assumed to be fabricated from a single homogeneous material for which Poisson's ratio is 0.3.

Shell Wall Construction

Two types of wall construction are treated, honeycomb sandwich and internally ring-stiffened monocoque.

Honeycomb sandwich wall.— The honeycomb sandwich wall is assumed to be symmetrical, i.e., having equal thickness face sheets, with uniform face sheet and core thicknesses. The core density is assumed to be three percent of the density ρ of the face sheet material.

Ring-stiffened wall.— In this case the shell skin thickness is assumed to be uniform but interior ring size and spacing are variable. The interior rings are Z-section rings, each being of uniform thickness.

Range of Parameters

Three nominal dimensionless buckling pressures, viz. $p/E \times 10^7 = 2$, 10, and 50 are considered. Because of the possibility of optimum designs lying on minimum gage constraint boundaries, two base radii are considered, viz. 57 in. and 114 in. Minimum gages assumed are: 0.016 in. for sandwich face sheets and skin of ring-stiffened shells, 0.032 in. for the wall of tubular base rings, 0.010 in. for the wall of Z-section interior rings, and 0.125 in. diameter for interior ring attachment rivets.

METHOD OF STRUCTURAL SYNTHESIS

Design-Analysis Iteration Procedure

A practical design optimization procedure was developed for sandwich and ring-stiffened shells of revolution.* In this procedure, the design of the structure is coupled iteratively with an elastic stability analysis of the design. Thus, structural weight is minimized with respect to buckling failure, as opposed to a stress failure. This is in accordance with the fact that, in general, for lightly loaded shells the critical mode of failure is buckling.

The iteration procedure is illustrated schematically in Figure 2. In this chart, dashed arrows represent return paths of iteration loops. Boxes bordered with heavy lines represent steps using computer programs. The

* Although this study is concerned with cones, the design procedure may be applied to more general shells of revolution (see Refs. 4 and 5).

group of boxes lying within the broken dot-dash border represents the design of the shell interior (i.e., exclusive of the nose and base ring). As shown, this group applies only to ring-stiffened construction. For sandwich cones it is replaced by a manual design step. The shell design step for both constructions is discussed further below.

Base Ring Design

Previous studies (Refs. 1 and 6) have shown that the function of edge rings for conical and cylindrical shells of revolution is to suppress in-extensional buckling, for which $N = 2$ is the critical harmonic. The following additional results, demonstrated in Reference 1 for blunt conical shells, have been found to be valid for more general shells of revolution (Refs. 4 and 5). There exists a critical harmonic $N_c > 2$ for which the critical load attains a relative minimum. In this buckling mode there is relatively little deformation at the shell edges. Therefore, the corresponding critical load is insensitive to the stiffness of edge rings. On the other hand, for edge rings of insufficient stiffness the critical load attains an absolute minimum for $N = 2$, this mode being essentially inextensional.

For blunt truncated shells of revolution having a nose ring attached at the small end and a base ring attached at the large end, large buckling deformations occur at the base ring in the $N = 2$ mode. Therefore, the corresponding critical load is not a strong function of the nose ring stiffness but is directly related to the base ring stiffness. In fact, for tubular base rings, which are assumed for this study, this critical load is approximately proportional to the flexural rigidity of the base ring. Its extensional rigidity has little effect since there is negligible extension in this buckling mode.

Thus at low values of the flexural rigidity (EI) of the base ring, the shell buckles at low load into the $N = 2$ mode. As EI is increased, the mode shape remains essentially unaltered, but the buckling load increases in the same proportion until the critical load for the $N = 2$ mode equals the critical load for the $N = N_c$ mode. Further increases in EI are ineffectual since henceforth the shell buckles in the $N = N_c$ mode, which is unaffected by the base ring. This behavior suggests that the base ring flexural rigidity should be chosen so that the critical loads corresponding to $N = 2$ and $N = N_c$ are equal. As indicated by Box F of Figure 2, this criterion is incorporated into the optimum design procedure.

In order to achieve a minimum weight tubular base ring it is desirable to have as large a ratio of tube radius to thickness as possible. This ratio is limited by either

- 1) local instability of the tube wall (for moderately loaded rings),
- 2) local distortion of the tube cross section at the shell interface (for lightly loaded rings), or
- 3) minimum gage.

Initially, the tube R/t was determined so that at the design load the tube becomes locally unstable. For this calculation, the maximum combined hoop compressive stress in the tube was assumed to be uniformly distributed, and the axial stress buckling criterion for moderately long cylindrical shells of Reference 7 was applied. However, if this computed value is too large, one can expect that the tube will cease to behave in accordance with ring theory, which treats the cross section as a rigid element. If this occurs, the ring flexural rigidity required to suppress the $N = 2$ buckling mode will not be achieved. In order to avoid this possibility, a limit of $R/t = 125$ was imposed. An additional constraint on R/t is provided by the requirement of minimum gage for the tube wall, taken to be 0.032 in., and the required moment of inertia of the tube section.

Nose Ring Design

In contrast to the large deformations which occur at the base ring in the $N = 2$ mode of buckling, this mode has typically small deformations at the nose ring. Hence, for practical rings, the nose ring stiffness has negligible effect on the shell buckling load. Since the nose ring is typically in a state of hoop tension, its design is based on considerations of stress, fabrication, and local buckling due to axial compression.

Two types of nose rings are used, one for the sandwich shells and the other for the ring-stiffened shells. These are illustrated in Figure 1.

Sandwich shell nose ring.— It is assumed that the axial reaction force of the external pressure is uniformly distributed over a 0.20 in. width centered at the midpoint of the radial flange of the nose ring (Fig. 1). The thickness t_{cyl} is designed for incipient local buckling of the two inch cylindrical element, treated as a wide column, at the nominal design pressure. The thickness t_{fl} is designed for a maximum dimensionless bending stress (σ/E) of 0.007 in the radial flange, treated as a cantilever beam. For either thickness a minimum gage limit of 0.050 in. was imposed.

Ring-stiffened shell nose ring.— It is assumed that the axial reaction force of the external pressure is uniformly distributed over the full radial element of the ring. The section modulus of the radial element, treated as a simply supported beam, is designed for a maximum bending stress (σ/E) of 0.007. For reasons of fabrication feasibility, the neces-

sary section modulus is assumed to be provided by the combination of the uniform thickness t of the ring and a one inch wide washer plate of thickness t_{wash} (also having the maximum stress $\sigma/E = .007$) in contact with the radial element. As is seen in Figure 1, a washer plate was employed in only two of the six cases. In the buckling analysis of the shell the stiffness contribution of the washer plate was neglected, whereas its weight is included in the structural weights presented.

Shell Design

As noted earlier, the payload and base ring have negligible effect on the critical load of the shell for $N = N_c > 2$. On the other hand, for a given shell structure, the $N = 2$ critical load is effectively controlled by the base ring. These facts allow the decoupling of the design of the shell, excluding the end rings, from the design of the rings themselves. The procedure then is to design the shell interior so that its critical load for $N = N_c$ is the design load. This procedure, shown inside the broken dot-dash border of Figure 2, is described in the following sections for the two wall configurations. After this design is achieved, the base ring is designed in accordance with the principles stated earlier.

Sandwich cones.— The design step for the sandwich cones consists of a determination of the core depth t_c and face sheet thickness t_f of the symmetrical sandwich wall. The following two conditions, the second of which may be overridden by the minimum gage constraint $t_f \geq t_f^*$, are imposed on these variables:

- 1) Critical pressure level for general instability equals the design pressure, and
- 2) Equal weights of material in core and face sheets.

Condition (1) is based on a general instability correlation obtained for a combined loading of a uniform hydrostatic pressure and an axial tension equal to the resultant of the hydrostatic pressure acting on the capsule base. For this correlation, the following linear interaction formula, based on the results of Reference 8, was used.

$$p/p_o - .65 P/P_o = 1 \quad (1)$$

Substitution of the critical hydrostatic pressure and critical axial load for a sandwich cone, viz.

$$p_o = 4.2 E t_f t_c^{1.5} / \bar{L} \bar{R}_2^{1.5}$$

$$P_o = 13.2 E t_f t_c \cos^2 \alpha$$

and the relation $P = \pi r_b^2 p$ into Eq. (1) gives the relation

$$p/E = \gamma (t_f/r_b) (t_c/r_b)^{1.5} / [1 - \kappa (t_c/r_b)^{.5}] \quad (2)$$

where

$$\gamma = 4.2 r_b^{2.5} / L \bar{R}_2^{1.5}$$

and

$$\kappa = .155 \gamma / \cos^2 \alpha$$

For the specified shell geometry, $\gamma = 3.54$ and $\kappa = 2.2$. Using these values and inserting a correlation factor C in Eq. (2) gives

$$p/E = 3.54 C (t_f/r_b) (t_c/r_b)^{1.5} / [1 - 2.2 (t_c/r_b)^{.5}] \quad (3)$$

Condition (2) is based on a slight modification of an elementary minimization of the shell surface density, $2t_f \rho_f + t_c \rho_c$, subject to the buckling constraint for hydrostatic pressure, $t_f t_c^{1.5} = \text{constant}$. This results in an optimum core weight to face sheet weight ratio of 1.5. Condition (2) is a more practical design condition in that it results in thicker face sheets, lower stresses and in designs that are less affected by transverse shear deformations. The theoretical weight penalty incurred by using Condition (2) is only 2%.

For an assumed value of ρ_c/ρ_f (in this study, $\rho_c/\rho_f = .03$ was used) Condition (2) translates into a known value, say τ , of t_f/t_c (i.e., $\tau = \rho_c/2\rho_f$). Substituting this relation into Eq. (3) to eliminate t_f gives

$$t_c/r_b = .603 (p/CE\tau)^{.4} [1 - 2.2 (t_c/r_b)^{.5}]^{.4} \quad (4)$$

For a given correlation factor C (estimated from the results of the previous iteration, see Fig. 1) Eq. (4) is solved numerically for t_c , and hence t_f . If, however, t_f turns out to be less than the minimum gage t_f^* , then t_f is set equal to t_f^* and t_c recomputed from Eq. (3).

Ring-stiffened shells.—Whereas the design step for sandwich cones is relatively simple and performed manually, the corresponding step for ring-stiffened cones required the development of a design computer program.

In order to retain as much generality as possible, the shell geometry accepted by the program is not restricted to cones. Instead, blunt truncated shells of revolution of general meridional shape are treated (see Refs. 4 and 5, where the application of this program to tension shells is reported).

In some cases stringers are incorporated into a design to suppress excessive prebuckling deformations. The stringers are not subject to local instability because they are in tension. Since a relatively small weight of stringers is usually sufficient, stringer properties are not optimized, but are treated as known data by the design program.

The design variables considered by the program are:

- 1) Shell wall thickness (assumed uniform),
- 2) Ring locations,
- 3) Ring cross-sectional lengths (assuming uniform thickness Z-section interior rings with a nominal web-to-flange width ratio of 2.5*), and
- 4) Ring cross-sectional thicknesses.

Thus a total of $3M + 1$ variables are considered where M is the number of rings required. The following conditions are imposed on these variables:

- 1) Critical pressure for general instability equals the design pressure,
- 2) Critical pressure for instability of shell bays between rings equals design pressure,
- 3) Critical pressure for local instability of each interior ring equals design pressure, and
- 4) Relative increase (due to stiffening) in the local hoop flexural rigidity of the composite shell wall is proportional to the normal deflection of the general instability mode.

Condition (1) is based on the general instability correlation for ring-stiffened conical shells under uniform hydrostatic pressure obtained by Baruch and Singer (Ref. 10). This correlation, however, is based on uniform ring size and spacing. For the purpose of optimum design it was generalized by replacing the relative increase η in hoop flexural rigidity of the composite shell wall due to the rings by a weighted average value $\bar{\eta}$ and inserting a correlation factor C .

* This is very nearly the optimum ratio for local stability of a Z-section ring (cf. Ref. 9).

Additionally, to include variable pressure loading the buckling pressure in the correlation is replaced by a weighted average pressure \bar{p} . The resulting correlation is then:

$$\bar{p} = (.92 CEt^{2.5}/L\bar{R}_2^{1.5}) [(1 + \bar{\eta})^{.75} - (\bar{R}_2 t)^{.5} \bar{\eta}/L] \quad (5)$$

Since stiffening in the vicinity of maximum buckle amplitude will have the greatest effect on critical load, it is reasonable to weight η with the normal buckling deflection w . The lowest power of w which will serve this purpose is 2, since additional stiffening must always increase the value of $\bar{\eta}$. The same argument may be applied to the pressure distribution so that the following average values are used.

$$\bar{\eta} = \int_S \eta w^2 ds / \int_S w^2 ds \quad (6a)$$

$$\bar{p} = \int_S p w^2 ds / \int_S w^2 ds \quad (6b)$$

For more general shells of revolution Eq. (5) is still used, but with a generalized definition of the average radius of curvature \bar{R}_2 . Comparison of the membrane hoop force equations for a cone and a more general shell of revolution suggests the following value for \bar{R}_2 .

$$\bar{R}_2 = [1/(r_b - r_a)] \int_{r_a}^{r_b} \{1 + [(r_b/r)^2 - 1](r/R_1)/[2(r/R_2)]\} [r/(r/R_2)] dr \quad (7)$$

For a cone, $r/R_1 \equiv 0$ and $r/R_2 \equiv \cos\alpha$, so that Eq. (7) reduces to

$$\bar{R}_2 = (r_b + r_a)/2\cos\alpha$$

It should be noted, however, that the application of Eq. (5) to shells with nonzero Gaussian curvature is an expedient in lieu of more valid instability correlations, such as might be obtained from the analysis of Reference 11.

Condition (2) is based on a treatment of the shell bays as wide simple supported plates. As shown in Reference 12, for sufficiently long shells with positive Gaussian curvature, the curvature may contribute additional buckling strength, whereas for shells with negative Gaussian curvature this effect tends to be small. In either case, for sufficiently short bays, as generally occur for optimum designs, the effect of curvature is negligible. On the other hand, the beneficial effect of meridional tension is included in the plate buckling formula according to (Ref. 13)

$$k_2 = 2[1 + (1 - k_1)^{.5}] \quad (8)$$

where the compressive stress coefficients k_1 and k_2 are given by

$$k_{1,2} = T_{1,2} d^2 / \pi^2 D$$

Condition (3) is based on the critical stress criterion for local instability of Z-section rings given in Reference 9. This may be written as

$$\sigma = 10.85 E(h/\ell)^2$$

As may be seen from the results of Reference 1, interior rings for lightly loaded ring-stiffened shells have negligible bending in the prebuckling state. Therefore, the criterion for local ring buckling is taken simply as*

$$T_\phi = 10 E h^3 / \ell \quad (9)$$

The ring hoop forces T_ϕ , as well as the local meridional and hoop shell skin forces T_1 and T_2 , are determined from membrane theory as functions of h , ℓ , d , and t (see Appendix A). In the membrane analysis, normal force equilibrium is written for a finite shell element (of width d) centered at a ring. It is assumed that variables in the membrane equations apply at the center of the element, i.e., at the ring. Variables required (shell geometry, pressure, and ring and stringer properties) to compute T_1 and T_2 for the bay buckling criterion are taken as mean values over the bay. These assumptions are valid only if these variables are slowly varying over each bay. Otherwise, a design will be obtained which may be locally unstable in

* The factor 10.85 was truncated to 10 as a small factor of conservatism. Additional conservatism is, of course, implied by the neglect of the shell wall restraint on the riveted flange of the ring.

certain regions. If this occurs, a fictitious pressure distribution with the pressure locally increased in the unstable regions (and possibly decreased in regions with a large stability margin) is input to the design program in the next design step. (See Box D in Fig. 2.)

The fourth condition is motivated by the desire to place the ring material where it will do the most good. It also allows a very important simplification of the design problem. For a given shell skin thickness t , Condition (1), through Eq. (5), dictates the necessary value of $\bar{\eta}$. Condition (4) may be written as

$$\eta = k|w| \quad (10)$$

where w is normalized with, say, its maximum value equal to unity. Substitution of Eq. (10) into Eq. (6a) gives

$$k(t) = \bar{\eta} \int_S w^2 ds / \int_S |w|^3 ds \quad (11)$$

Since an approximation to w is known from the previous iteration (cf. Fig. 2), Eqs. (5) and (11) give k as a function of the shell thickness t .

In general, the value of η at an interior ring is given by*

$$\eta = E_R I_e / Dd + 12(e/t)^2$$

Here the hoop flexural rigidity of the composite wall is taken about the centroid of the ring-shell combined section. For a Z-section ring with a web-to-flange ratio of 5/2, η is given as a function of h , ℓ , d , and t by

$$\eta = \{ .0343(1-\nu^2)(E_R/E)h\ell^3[17(h\ell+td)^2 + 27t^2d^2] + .926 h^2\ell^4td \} / t^3d(h\ell+td)^2 \quad (12)$$

Thus, since for a given shell thickness, T_1 , T_2 , T_ϕ , and η are known functions of h , ℓ , and d , Conditions (1), (2), and (3), as represented by Eqs. (5), (8), and (9), can be used to solve for each interior ring (i.e., h and ℓ) and its spacing (i.e., d) in sequence.† In effect, a nonlinear problem with 3M degrees of freedom is reduced to a sequence of M problems, each of which, although still nonlinear, has only three degrees of freedom.

For an assumed shell thickness, the solution for each ring is illustrated schematically in Figure 3. For a given value of d , each curve divides the h - ℓ plane into a stable region (to the right) and an unstable region (to

* In general, the interior rings need not be of the same material as the shell skin.

† In so doing, Eqs. (10), (11), and (12) are used with Eq. (5), Eqs. (A7) and (A8) are used with Eq. (8), and Eq. (A9) is used with Eq. (9).

the left). In order to be stable with respect to the criteria of Eqs. (5), (8), and (9), a design point must lie to the right of all three curves. The criterion for determining where the solution point should lie within the stable region is that the added ring volume per unit of surface area ($h\ell/d$) should be a minimum. If this condition is met for each ring, then it is clear that for the shell thickness considered, the design is optimum. The following properties of the curves of Figure 3 can be proven:

- 1) On S, $\partial(h\ell)/\partial h > 0$,
- 2) At the intersection of S and R, $\partial(h\ell/d)/\partial d < 0$ and $\partial h/\partial d > 0$, and
- 3) On B, $h\ell = \text{const.}$ and $\partial(h\ell/d)/\partial d > 0$.

It is clear from Property (1) that for a given low value of d [Fig. 3(a)] the optimum point is the intersection of the curves S and R. Because of Property (2), $h\ell/d$ can be decreased by increasing d until the three curves have a common intersection. However, because of Property (3), a further increase in d will cause $h\ell/d$ to increase. Therefore, the simultaneous solution of Eqs. (5), (8), and (9), represented by the common intersection in Figure 3(b) is, indeed, the optimum solution.

In order to insure fabrication feasibility, after each solution depicted in Figure 3(b) is obtained, it is examined and, if necessary, altered in accordance with the following manufacturing constraints built into the program:

- 1) Minimum rivet diameter, $d_r \geq d_{r_{\min}}$,
- 2) Minimum ring gage, $h \geq h_{\min}$, and
- 3) Riveted flange constraints, $4d_r \leq f_R \leq d/2$.

The rivet diameter d_r is computed according to

$$d_r = \text{Max} (4\tilde{t}, d_{r_{\min}}) \quad (13)$$

where

$$\tilde{t} = \text{Min} (t, h) \quad (14)$$

The estimate $4\tilde{t}$ for the rivet diameter is based on equality of bearing strength of the minimum thickness sheet and the shear strength of the rivet.[†]

[†] Strictly speaking, the estimate $4\tilde{t}$ results in the stated equality only if the ratio of ultimate bearing stress of the sheet to the ultimate shear stress of the rivet is π . Since this equality is not fundamental to the design, this estimate of rivet diameter, which is reasonable, is used in all cases.

If then $4d_r \leq d/2$, Constraints (2) and (3) are imposed without changing the computed ring spacing d . Note that before imposing the constraints, $f_R = 2\ell/9$. If $h < h_{\min}$ or $2\ell/9 > d/2$ the solution point is moved from the common intersection in Figure 3(b) along the curve S down and to the right until the violated condition is satisfied. This results, of course, in increased weight (cf. Property (1) above). If, on the other hand, $\Delta = 4d_r - 2\ell/9 > 0$, then f_R is simply increased by the amount of Δ without changing the ring thickness or widths of the ring web or free flange. In this event, $f_R > 2\ell/9$, and Figure 3, being based on rings with proportions of 2.5 to 1, no longer applies. However, the addition of this material cannot weaken the design.

On the other hand, if $4d_r > d/2$, then it is necessary to pay the penalty of increasing d above the optimum value. In this case, d is set equal to $8d_r$ and Figure 3(c) then applies. In this condition, the constraints are reduced in number to two, viz. $h \geq h_{\min}$ and $f_R = d/2$. In Figure 3(c), the minimum weight stable design lies on the segment OP of the curve B bordering the stable region, along which $h\ell/d$ is constant. However, as before, if $h_1 < h_{\min}$ or $\ell_1 > 9d/4$, it is necessary to move to a point on the portion of the curve S bordering the stable region. Otherwise, the solution is chosen on OP with the largest value of ℓ (and consequently, the smallest value of h) consistent with the conditions $h \geq h_{\min}$ and $2\ell/9 \leq d/2$. As before, in either case, it still may be necessary to increase f_R by the amount $\Delta = 4d_r - 2\ell/9$.†

Following the above-outlined procedure, the design program obtains successively optimized ring size and spacing distributions for several shell thicknesses. The initial shell thickness and a thickness increment are input quantities, along with shell geometrical data, shell and ring material properties, extensional rigidity of stringers, pressure distribution, load factor, minimum ring gage, minimum rivet diameter, general instability correlation factor, and an estimate of the normal deflection function of the general instability mode. For each shell thickness the total structural weight, including shell skin, interior rings, and an estimate for rivet weight,§ is computed. The process is terminated after the total structural weight attains a relative minimum with respect to shell thickness.

† It is noted that since d_r depends on h through Eqs. (13) and (14), in practice, satisfaction of the constraints is an iterative process.

§ The estimated rivet weight is based on the following assumptions for each interior ring: 1) if $f_R < 8d_r$, there is one circumferential row of rivets, whereas if $f_R \geq 8d_r$, there are two rows; 2) for each row the rivet spacing is $20t$; 3) the rivet density is equal to the ring density; and 4) the two heads of each rivet have a total volume of $0.816 \pi d_r^3$.

Shell Analysis

The shell design procedures, discussed in the preceding sections, are based on certain approximations, which require verification and, if necessary, modification by more precise analytical methods. With regard to the sandwich cones, this involves a straightforward calculation of the prebuckling state and corresponding critical load, as shown in the boxes labeled B and E in Figure 2. The prebuckling states were computed according to nonlinear moderate rotation theory using a computer program which extends the axisymmetric linear solution of Reference 14 by Newton's method. The stability analyses (Boxes E and F in Figure 2) were carried out using the computer program discussed in Reference 15. Since uniform live normal pressure is nonconservative for shells with edge rings, the stability analyses are based on dead pressure loading.*

The above discussion applies also to the ring-stiffened designs, except that, because of the relatively large number of rings required, it was convenient to analyze modified designs having a different number of rings, rather than the actual designs obtained. This modification consists of the replacement of the actual discrete ring distribution by an equivalent modified discrete ring distribution at a set of modified ring locations. One or more actual rings are lumped at the nearest modified ring location, thus forming a modified ring having extensional, flexural, and torsional rigidities equal to the sum of these rigidities of the component rings and a normal eccentricity equal to the average of the eccentricities of the component rings. The set of modified ring locations is sufficiently dense (up to 31 points were used) so that, insofar as the actual design has sufficiently many rings to be analyzed on a "smeared-out" ring stiffness basis, with respect to general instability the modified design and the actual design are equivalent.

On the other hand, with respect to bay and local ring instability, the modified design clearly does not model the actual design. Therefore, to check these modes of buckling, it was necessary to employ an additional program represented by Box C in Figure 2. This program uses as input the prebuckling stress resultants computed for the modified design (in step B of Figure 2), and is based on the assumption that the total circumferential (including rings) and meridional (including stringers) stress resultants are approximately the same for both modified and actual designs. Employing strain compatibility between shell, rings, and stringers (neglecting their eccentricities), it computes the shell and ring stress resultants at the design load. These are compared to the buckling allowables for all shell bays and interior rings, given by Eqs. (8) and (9), respectively. If local instability is found, the design is iterated through the boxes D, A, and B.

*See Reference 1 for an assessment of this effect.

RESULTS

Sandwich Cones

In Table I are presented the essential results of the sandwich cone designs. In this table the critical harmonic number is given in parentheses following the dimensionless buckling pressure. Typically, as the design pressure increases, the critical harmonic number decreases.

The dimensionless weights shown are ideal weights including face sheets, core, and edge ring weights, but excluding adhesive bond and other necessary fabrication weights. Since the adhesive weight is essentially independent of design pressure and varies as the shell surface area, it would have its greatest relative effect on dimensionless weight at low design pressure and, particularly, for small base radii. As is shown, the sandwich face sheets are minimum gage for Cases 1 through 4, whereas the base rings are minimum gage for Cases 1, 2, and 4. On the other hand, the R/t ratios of the Case 3, 5, and 6 base rings are local buckling limited. As a result of the minimum gage constraints, the larger designs have lower dimensionless weights than the smaller designs. In order to facilitate the estimation of structural weight for other sizes and loadings, algebraic correlations of the results of Table I are presented in Appendix B.

The prebuckling states for these designs are shown in Figures 4 through 9. Also shown by the dashed line in these figures is the dimensionless hoop stress resultant, $pR_2/r_b E \times 10^7$, predicted by membrane theory. As the design pressure increases, the region of validity of the membrane theory becomes progressively smaller until, at $p/E = 50 \times 10^{-7}$, membrane conditions are attained nowhere. The effect of shell bending is to increase algebraically the circumferential stress resultant, thereby resulting in a buckling pressure greater than that predicted by membrane theory.

The corresponding buckling modes are shown in Figures 10 through 15.* Comparison of these figures shows that the buckling mode shape is rather insensitive to the design pressure or size. There is, however, some tendency for the tangential buckling deflections to grow with increasing design pressure.

*The $N = 2$ buckling modes, being characteristically linear with maximum deflection at the shell base (Refs. 1 and 4), are not shown.

Ring-Stiffened Cones

In Table II are presented the essential elements of the ring-stiffened cone designs. As is true for the sandwich cones, the critical harmonic number (given in parentheses after the critical pressure) decreases as the design pressure increases.

In this case, the dimensionless weights shown include, in addition to shell skin and ring weights, a weight estimate for the interior ring attachment rivets. Thus these weights are not directly comparable to the sandwich weights (Table I), since the sandwich weights do not include adhesive bond weight. The Case 4 and 5 designs utilize 30 ($.5 \times .75 \times .1 \times .010$ in.) internal stringers, which run the full length of the cone and are equispaced around the shell circumference. The small dimensionless weight (0.024×10^{-3}) of these stringers is also included in the weights shown for Cases 4 and 5 in Table II. Stringers are employed because for these very thin shells ($r_b/t = 4385$ and 3353) the method of forward integration used in the numerical analysis requires in the mathematical model more than the 33 subintervals currently dimensioned in the analysis computer programs. Since a small amount of stringers has the beneficial effect of reducing prebuckling rotations as well as the required number of subintervals and may, in fact, produce a more optimum design, they were incorporated into these designs.

In contrast to the sandwich designs, in no case is the skin thickness minimum gage. However, the constraints of minimum interior ring gage and minimum rivet diameter limit all the designs except Cases 3 and 6, as shown in the following table.

<u>Case</u>	<u>No. min. gage int. rings</u>	<u>No. int. rings with min. gage rivets</u>
1	all	all
2	none	all
3	none	none
4	1	all
5	none	3
6	none	none

Since the Case 3 shell is unconstrained by minimum gage, the Case 6 shell interior is identical to it except for scale. With respect to the base rings, Cases 1 through 4 are minimum gage, whereas for Cases 5 and 6 the base ring R/t ratios are limited to 125. Consequently, although the Case 3 and Case 6 shell interiors scale, their base rings do not. In contrast to the sandwich designs, none of the ring-stiffened cone base rings is local stability critical.

In general, the number of interior rings decreases with increasing design pressure. As seen from Table II, minimum gage constraints can reverse this relationship. Interior ring locations and their dimensions for Cases 1 through 5 are shown in Tables III through VII, respectively.

As noted earlier, the buckling pressures shown are based on nonlinear prebuckling states. The effect of nonlinearity was checked for Cases 1, 2, and 3, and, as expected, was found to have its greatest effect for the high pressure design, Case 3. In general, the effect of nonlinearity is to increase the buckling pressure. The percent increases for Cases 1, 2, and 3 are 2.0%, 3.2%, and 11.4%, respectively.

The prebuckling states for the corresponding modified structures (cf. Shell Analysis, p. 18) are shown in Figures 16 through 20, respectively. Note that Figure 18 applies for all base radii greater than or equal to 57 in. Superimposed on these figures are the shell hoop stress resultant distributions computed for the actual structure from Eq. (A8) of Appendix A. For the low pressure designs (Figs. 16 and 19), the difference between Eq. (A8) and the hoop force for the modified structure is negligible over most of the shell interior. The greatest discrepancy occurs for the high pressure design (Fig. 18). The ring rotation tends to reduce the compressive hoop stress in the rings and to increase the compressive hoop stress in the shell skin. Therefore, it is probable that the Case 3 design is underdesigned for local bay buckling and overdesigned for local ring buckling. However, because these two effects are compensating, the resulting error in the optimum structural weight is probably small.

The buckling mode shapes for the ring-stiffened designs are shown in Figures 21 through 25. In contrast to the sandwich cones, there is some tendency for the location of maximum buckle amplitude to move aft with increasing design pressure. In these figures the normalized mass distribution (i.e., the surface density $\rho A_R/d$) of the interior rings is superimposed on the normal deflection shape of the buckling mode. In practice, the average distribution of the normal deflection of several buckling modes is input to the design program. This is done in order to avoid weakening the shell with respect to one mode while stiffening it with respect to another. As a result of the minimum gage constraints the deviation of the ring mass distribution from the normal deflection shape is greatest for the Case 1 design (Fig. 21). However, it should be noted that it is not desired to make the ring mass distribution (which corresponds to an increase in local hoop extensional rigidity of the composite shell wall) proportional to the buckling mode, but rather the flexural rigidity function η (cf. Shell Design, p. 15).

In order to assess the benefit gained by the additional design degrees of freedom associated with variable ring size and spacing, dimensionless weights for shell wall and interior rings were computed for the Case 4, 5, and 6 critical pressures (see Table II) using the approximate analysis of

Burns (Ref. 2) for equally spaced identical rectangular rings. In order to be able to realistically compare the results of this calculation with the corresponding weights for the present designs, it is necessary to assess also three basic causes of difference in these results other than the one of interest. These are: (1) the use of rectangular interior rings in Reference 2 versus the use of the more efficient Z-section rings in this study; (2) the assumption of hydrostatic pressure loading in Reference 2 versus the assumption of the less stringent lateral pressure loading in this study; and (3) the error in the approximate formulas of Reference 2, which to some extent compensates for the first and second assumptions. The differences caused by these assumptions are estimated and then applied to correct to first order the weights predicted by Burns' approximate analysis to the same basis as the present results.

Based on the efficiency factors given in Reference 2, the use of Z-section rings would result in a weight saving of approximately 9.4%. Also, if the local bay buckling criterion is based on lateral pressure (i.e., use of a plate buckling coefficient of 4 instead of 2), the approximate analysis predicts an additional weight saving of 8.4%. On the other hand, a first order estimate of the error in the approximate analysis of Reference 2 indicates that for Cases 4, 5, and 6 it underestimates the weights by 7.2%, 9.6%, and 12.5%, respectively. The table below compares the total weight for the shell and interior rings obtained from the approximate analysis of Reference 2 with the corresponding weights (excluding rivet weight) from this study.

$\frac{W/\rho r_b^3 \times 10^3}{\text{---}}$					
Case	$p/E \times 10^7$	This Study	Ref. 2	Weight Ratio	Corrected Weight Ratio
4	1.86	0.96	1.33	1.39	1.24
5	9.28	2.24	3.17	1.42	1.29
6	43.15	5.81	7.25	1.25	1.16

The imposition of manufacturing constraints in the present study, which affect Case 4 and, to a lesser degree, Case 5, has reduced the weight ratios shown for these cases.* This fact, coupled with the differences shown, suggests that the relative weight saving to be gained by allowing variable ring size and spacing increases with decreasing design pressure.

*Since the various modes of buckling have not been checked for the design equations of Reference 2, it is probable that additional modification of the weights predicted by them is required to compensate for the approximate nature of the underlying assumptions used.

Singer, et al. (Ref. 3) presents results for a 120° cone for $p/E = 6 \times 10^{-7}$ and $r_a/r_b = 0.25$. For the ring spacing law $d \propto 1/r \cdot .5$, corresponding ideally to equal strength bays, they report an optimum weight for shell plus interior rings of $W/\rho r_b^3 = 2.84 \times 10^{-3}$. For equally spaced rings the optimum weight is increased only slightly to 2.94×10^{-3} . On the other hand, Burns' approximate analysis for equally spaced rings gives for this shell $W/\rho r_b^3 = 2.62 \times 10^{-3}$. This discrepancy is caused primarily by the more stringent assumption in Reference 3 regarding the shell skin stress, viz. that the full hydrostatic membrane stress is developed in the shell skin.

Configuration Comparison

In Figures 26 and 27 the dimensionless structural weights given in Tables I and II are plotted versus dimensionless buckling pressure. As noted, these curves are not directly comparable since the sandwich cone weights exclude the adhesive bond weight, whereas the ring-stiffened cone weights include the (analogous) rivet weight for the interior rings. In spite of this bias, ring-stiffened construction is seen to be lighter in the low pressure range, whereas sandwich construction is lighter in the high pressure range. This inversion of relative standing with pressure variation is primarily a result of minimum gage constraints (which, of course, also cause the dependence of dimensionless weight on base radius). As shown in Tables I and II, the sandwich cone face sheets are minimum gage in Cases 1 through 4, whereas the optimum ring-stiffened cone skin thickness is always greater than minimum gage. Since the sandwich adhesive weight is essentially independent of design pressure and is proportional to the square of the base radius, it also has its greatest relative effect on dimensionless weight at low loading and small size, thereby accentuating the effect of minimum gage. For example, if one assumes an adhesive weight of 0.2 lb/ft^2 of surface area and a structural density of 0.1 lb/in^3 , then $W/\rho r_b^3 \times 10^3$ should be increased by 0.39 and 0.78 for $r_b = 114$ and 57 in. , respectively. Adding these amounts to the curves of Figure 26 and comparing the resulting curves with those of Figure 27, as shown in Figure 28, one concludes that, under these assumptions, ring-stiffened construction is lighter for $p/E \times 10^7 < 8.5$ and 18.0 for $r_b = 114$ and 57 in. , respectively.*

In order to illustrate the degree of optimization achieved, the sandwich and ring-stiffened cone designs of Reference 1 are represented in Figures 26 and 27, respectively, as small circles. These designs are also 120° cones, but have a truncation radius ratio of 0.445 . The values shown for these designs have been corrected approximately to the ratio $r_a/r_b = 1/3$ in order to be consistent with results of this study. For this weight

*Including the additional weights associated with edge closure and core inserts for the sandwich wall would increase further these inversion pressures.

calculation the base rings were chosen, as in this study, so that the $N = 2$ critical pressure equals the higher harmonic critical pressure. It is noted that the sandwich design of Reference 1 is not homogeneous, having an aluminum shell and magnesium edge rings. The dimensionless weight shown for the sandwich shell is based on the density of aluminum, 0.1 lb/in.^3 . The ring-stiffened cone is homogeneous (of magnesium) and has equally spaced identical tubular interior rings. Since the base radius of these shells is 90 in., it is evident from Figures 26 and 27 that they are both nonoptimum designs. Relative to these designs, a much greater degree of optimization was achieved for the ring-stiffened shell than for the sandwich shell. In fact, the apparent conclusion of Reference 1, that for $r_b = 90 \text{ in.}$ and $p/E \times 10^7 \approx 6$, sandwich construction is superior, has now been reversed (cf. Fig. 28).

Also shown by the small triangles in Figures 26 and 27 are the low temperature (300°F) sandwich and ring-stiffened 120° conical aeroshell weights of Reference 4.* They have been corrected approximately to the present truncation radius ratio of $1/3$, and, in addition, weight allowances for splices, tube support, sandwich closure, and heat shields have been subtracted out. Since these designs are based on variable pressure loading, their weights are plotted for a mean value of pressure, taken to be 1.73 psi on the scale of Figure 11 of Reference 4. It is noted that, based on this mean pressure value, the sandwich capsule results are in excellent agreement with the present results, whereas the ring-stiffened capsule weights are greater by 3.4% for the low pressure design and 7.9% for the high pressure design. The improvement obtained in the present designs results essentially from three beneficial effects considered here but not in Reference 4. These are: (1) the nonlinearity of the prebuckling state (cf. p. 21), (2) the meridional tension in the bay buckling criterion, and (3) the inclusion of a small amount of stringers in the Case 4 and 5 designs.

Another point of comparison with the results of Reference 4 is the inversion pressure, below which ring-stiffened designs are optimum, predicted by the present results. Design pressure is approximately proportional to ballistic coefficient for entry capsules, and for entry from orbit into the Martian atmosphere this relation is

$$p \text{ (psi)} \approx 19.5 \beta \text{ (slug/ft}^2\text{)}$$

which includes a factor of safety of 2.25. Based on the inversion pressures of $8.5 \text{ E} \times 10^{-7}$ and $18.0 \text{ E} \times 10^{-7}$ given earlier and a Young's modulus for aluminum at 300°F of $9.35 \times 10^6 \text{ psi}$, one concludes that ring-stiffened construction is optimum for ballistic coefficients less than 0.41 and 0.86 slug/ft² for 19 and 9.5 foot diameter capsules, respectively. Thus the result of Reference 4, that for 19 foot diameter capsules, ring-stiffened construction is optimum for ballistic coefficients less than 0.42 slug/ft² has been extended to smaller capsule sizes.

*These weights correspond to capsule designs with ballistic coefficients of 0.32 and 0.64 slug/ft² for entry at orbital speeds into the Martian atmosphere.

CONCLUDING REMARKS

A practical optimum design procedure for buckling limited shells of revolution has been presented. The procedure is essentially an automated one, being based on computer analysis and (for ring-stiffened shells) computer design. In this study this procedure has been used to obtain feasible point designs for sandwich and ring-stiffened 120° truncated conical shells. Designs are presented for a wide range of critical pressures and, in order to evidence the effect of minimum gage, two base radii.

The main conclusion to be drawn from the results of this study is that, for optimized designs, ring-stiffened construction is structurally superior to sandwich construction for lightly loaded shells. This is an important result since it is in agreement with the practical desirability of ring-stiffened construction over sandwich construction. The weight curves presented for both constructions may also be useful in future system trade-off studies of geometrically similar planetary entry capsules.

The optimum design computer program developed for this task represents an engineering approach to a complex mathematical programming problem. Its successful application to cones suggests the possibility of applying it to more general shells of revolution (cf. Refs. 4 and 5). A major difficulty in this regard is the nonavailability of shell instability correlations. Additional research, possibly along the lines of Reference 11, is evidently needed in this area.

APPENDIX A

DETERMINATION OF STRESS RESULTANTS OF RING-STIFFENED SHELLS USING MEMBRANE THEORY

Normal force equilibrium is written for a finite shell element of width d centered at an interior ring, i.e.,

$$(T_1 + \Delta T_1)/R_1 + (T_2 + T_\phi/d)/R_2 = p \quad (A1)$$

It is assumed that all variables appearing in Eq. (A1) are slowly varying over the element so that this equation is valid when these variables are evaluated at the midpoint of the element (i.e., at the ring). Axial force equilibrium gives

$$T_1 + \Delta T_1 = -pz \quad (A2)$$

where
$$z = \int_r^b pr dr / pr(r/R_2)$$

These equations are supplemented by the membrane constitutive relations for shell, rings, and stringers, viz.

$$\epsilon_1 = (T_1 - \nu T_2)/Et \quad (A3)$$

$$\epsilon_2 = (T_2 - \nu T_1)/Et \quad (A4)$$

$$T_\phi = (EA)_R \epsilon_2 \quad (A5)$$

$$\Delta T_1 = n(EA)_S \epsilon_1 / 2\pi r \quad (A6)$$

in which compatibility of strains (neglecting ring and stringer eccentricities) is implicit. Equations (A1) through (A6) are six equations in six unknowns which have the solution

$$T_1 = -pR_2 [(1 + x)z/R_2 - \nu y(1 + z/R_1)]/T \quad (A7)$$

$$T_2 = pR_2 [(1 + y)(1 + z/R_1) - \nu xz/R_2]/T \quad (A8)$$

$$T_\phi = pR_2 x d \{ [1 + (1 - \nu^2)y](1 + z/R_1) + \nu z/R_2 \} / T \quad (A9)$$

where

$$x = (EA)_R / Etd$$

$$y = n(EA)_S / 2\pi Etr$$

$$T = (1 + x)(1 + y) - v^2 xy$$

APPENDIX B

SANDWICH CONE CORRELATIONS

Least square correlations of the results presented in Table I are derived in this appendix.

Base Ring

For the six base rings of Table I, the dimensionless flexural rigidity EI/pr_b^4 varies only slightly. For Cases 1 through 6 respectively, EI/pr_b^4 takes the values: 0.117, 0.110, 0.118, 0.117, 0.116, and 0.124. Taking the mean, 0.117, of these values, one obtains the correlation

$$I/r_b^4 = .117 p/E \quad (B-1)$$

Equation (B-1) gives the minimum base ring moment of inertia required to suppress the $N = 2$ buckling mode.

For the three unconstrained base rings, Cases 3, 5, and 6, the following least square correlation for the dimensionless section area may be obtained

$$A/r_b^2 = 3.55(p/E)^{.75} \quad (B-2)$$

Equation (B-2), which fits these three data points with less than one percent error, reflects the local stability limit of tubular base rings. Equations (B-1) and (B-2) are two equations for the two base ring variables R and t . They have the solution

$$R/r_b = .257(p/E)^{.125} \quad (B-3)$$

$$t/r_b = 2.20(p/E)^{.625} \quad (B-4)$$

Equation (B-2) also yields the unconstrained base ring weight correlation

$$W/\pi p r_b^3 = 7.10(p/E)^{.75} \quad (B-5)$$

Equation (B-5) is valid if t , obtained from Eq. (B-4), is greater than or equal to the minimum gage t_{\min} . On the other hand, if $2.20(p/E)^{.625} < t_{\min}/r_b$, then Eq. (B-2) is replaced by the constraint $t = t_{\min}$, in which case Eq. (B-1) gives

$$R/r_b = .334 (p r_b / E t_{\min})^{.333} \quad (B-6)$$

and the ring section area is

$$A/r_b^2 = 2.10 [(p/E)(t_{\min}/r_b)^2]^{.333} \quad (B-7)$$

Equation (B-7) yields the constrained base ring weight correlation

$$W/\pi p r_b^3 = 4.20 [(p/E)(t_{\min}/r_b)^2]^{.333} \quad (B-8)$$

In practice, if only the base ring weight is desired, it is not necessary to refer to Eq. (B-4) since the larger of Eqs. (B-4) and (B-8) always applies.

Sandwich Shell

The sandwich shell results presented in Table I are correlated with Eq. (2). The constants γ and κ were determined so that Eq. (2) fits the six data points of Table I with minimum square error. The result is $\gamma = 5.35$ and $\kappa = 4.10$, which fit the data with a maximum error of 11 percent.* For shells unconstrained by minimum gage, the design condition of equal core and face sheet weights gives

$$t_f/t_c = \rho_c/2\rho_f \equiv \tau \quad (B-9)$$

Substituting Eq. (B-9) and the above values of γ and κ into Eq. (2) and solving (approximately) for t_c gives

$$t_c/r_b = .542 x(1 - 1.20 x^{.5}) \quad (B-10)$$

$$x = [(p/E\tau)(1 - r_a/r_b)]^{.4}(1 + r_a/r_b)^{.6}$$

From Eq. (B-9) one obtains the unconstrained shell weight correlation

$$W/\pi p r_b^3 = 4.62 \tau [1 - (r_a/r_b)^2] t_c/r_b \quad (B-11)$$

Equations (B-10) and (B-11) are valid if t_f , from Eq. (B-9), is greater than or equal to the minimum gage $t_{f\min}$. Otherwise, Eq. (B-9) is replaced by the constraint $t_f = t_{f\min}$. In this case Eq. (2) gives approximately

$$t_c/r_b = .361 y(1 - 1.64 y^{.5}) \quad (B-12)$$

where $y = [(p/E)(1 - r_a/r_b)(r_b/t_{f\min})]^{.667}(1 + r_a/r_b)$

The constrained shell weight is then given by

$$W/\pi p r_b^3 = 2.31 [1 - (r_a/r_b)^2](\tau t_c/r_b + t_{f\min}/r_b) \quad (B-13)$$

*In order to allow the best possible fit of Eq. (2) to the computer results, both constants γ and κ were allowed to vary from their theoretical values (See p. 11).

REFERENCES

1. Cohen, G. A.: The Effect of Edge Constraint on the Buckling of Sandwich and Ring-Stiffened 120 Degree Conical Shells Subjected to External Pressure. NASA CR-795, 1967.
2. Burns, A. B.: Minimum-Weight Hydrostatically Compressed, Ring-Stiffened Cones. J. Spacecraft Rockets, vol. 3, no. 3, March 1966, pp. 387-392.
3. Singer, J.; Berkovits, A.; Weller, T.; Ishai, O.; Baruch, M.; and Harari, O.: Experimental and Theoretical Studies on Buckling of Conical and Cylindrical Shells under Combined Loading. TAE Report 48, Technion Research and Development Foundation, Haifa, Israel, June 1966, Section 4.
4. Cohen, G. A.; Foster, R. M.; and Dowty, J. R.: Synthesis of Optimum Structural Designs for Conical and Tension Shell Mars Entry Capsules. NASA CR-1365, 1969.
5. Cohen, G. A.: Evaluation of Configuration Changes on Optimum Structural Designs for a Mars Entry Capsule. NASA CR-1414, 1969.
6. Cohen, G. A.: Buckling of Axially Compressed Cylindrical Shells with Ring-Stiffened Edges. AIAA J., vol. 4, no. 10, October 1966, pp. 1859-1862.
7. Anon.: NASA Space Vehicle Design Criteria - Buckling of Thin-Walled Circular Cylinders. NASA SP-8007, 1965.
8. Seide, P.: The Stability of Thin Conical Frustums Subjected to Axial Compression and Internal or External Uniform Hydrostatic Pressure. AFBMD-TR-61-37, March 1961.
9. Steinbacher, F. R.; and Gerard, G.: Aircraft Structural Mechanics. Pitman Publ. Corp., 1952, p. 271.
10. Baruch, M.; and Singer, J.: General Instability of Stiffened Circular Conical Shells under Hydrostatic Pressure. Aeron. Quart., vol. 16, May 1965, pp. 187-204.
11. Kan, S. S.: Stability of Shells of Revolution with Arbitrary Generatrix Curvature. PMM (Russian), vol. 2, 1966, pp. 36-43 (ITIS translation FTD-HH-66-786).
12. Stein, M.; and McElman, J. A.: Buckling of Segments of Toroidal Shells. AIAA J., vol. 3, no. 9, September 1965, pp. 1704-1709.

13. Batdorf, S. B.; Stein, M.; and Libove, C.: Critical Combination of Longitudinal and Transverse Direct Stress for an Infinitely Long Flat Plate with Edges Elastically Restrained Against Rotation. NACA Wartime Rep. L-49, March 1946. (Originally issued as NACA ARR L6A05a.)
14. Cohen, G. A.: Computer Analysis of Asymmetrical Deformation of Orthotropic Shells of Revolution. AIAA J., vol. 2, no. 5, May 1964, pp. 932-934.
15. Cohen, G. A.: Computer Analysis of Asymmetric Buckling of Ring-Stiffened Orthotropic Shells of Revolution. AIAA J., vol. 6, no. 1, January 1968, pp. 141-149.

TABLE I
SANDWICH CONE DESIGNS

Case	r_b (in.)	$p/E \times 10^7$	$W/\rho r_b^3 \times 10^3$	Shell		Base Ring	
				t_f (in.)	t_c (in.)	R (in.)	t (in.)
1	57	2.00(8)	2.87	0.016	0.135	1.35	0.032
2	57	9.88(6)	3.67	.016	.379	2.25	.032
3	57	50.33(5)	6.13	.016	.869	3.21	.060
4	114	2.00(7)	1.70	.016	.449	3.40	.032
5	114	10.03(5)	2.72	.017	1.124	5.18	.045
6	114	49.57(5)	5.65	.027	1.827	6.52	.120

TABLE II

RING-STIFFENED CONE DESIGNS

Case	r_b (in.)	$p/E \times 10^7$	$W/\rho r_b^3 \times 10^3$	Shell		Base Ring	
				t (in.)	No. int. rings	R (in.)	t (in.)
1	57	2.27(6)	2.85	0.022	18	1.48	0.032
2	57	9.69(5)	4.03	.025	23	2.32	.032
3	57	43.15(4)	7.83	.038	16	3.69	.032
4 ^a	114	1.86(6)	1.66	.026	36	3.42	.032
5 ^a	114	9.28(5)	3.11	.034	35	5.20	.042
6	114	43.15(4)	7.54	.076	16	7.45	.060

^a These designs utilize 30 (.5 × .75 × .1 × .010 in.) full length stringers.

TABLE III

RING LOCATIONS & DIMENSIONS
RING STIFFENED CONE, CASE 1

RING NO.	r/r_b	h/r_b	ℓ/r_b	Δ/r_b
1	0.4073	1.754×10^{-4}	1.367×10^{-2}	5.733×10^{-3}
2	.4673	↓	1.539	5.352
3	.5191		1.623	5.165
4	.5652		1.690	5.017
5	.6071		1.733	4.922
6	.6457		1.754	4.873
7	.6814		1.754	4.874
8	.7148		1.766	4.847
9	.7462		1.748	4.888
10	.7760		1.727	4.935
11	.8043		1.701	4.993
12	.8315		1.674	5.051
13	.8577		1.660	5.084
14	.8831		1.614	5.184
15	.9076		1.518	5.398
16	.9312		1.445	5.561
17	.9543		1.386	5.692
18	.9766		1.147	6.222

TABLE IV
RING LOCATIONS & DIMENSIONS
RING STIFFENED CONE, CASE 2

RING NO.	r/r_b	h/r_b	ℓ/r_b	Δ/r_b
1	0.3912	3.410×10^{-4}	2.106×10^{-2}	4.093×10^{-3}
2	.4401	3.658	2.351	3.547
3	.4841	3.761	2.469	3.285
4	.5238	3.829	2.555	3.094
5	.5603	3.867	2.611	2.969
6	.5940	3.882	2.643	2.899
7	.6254	3.889	2.665	2.851
8	.6550	3.944	2.730	2.705
9	.6831	3.941	2.734	2.695
10	.7097	3.916	2.719	2.730
11	.7350	3.913	2.725	2.716
12	.7592	3.916	2.733	2.698
13	.7824	3.915	2.738	2.688
14	.8047	3.910	2.737	2.689
15	.8262	3.899	2.730	2.704
16	.8469	3.882	2.717	2.734
17	.8669	3.856	2.694	2.786
18	.8862	3.816	2.655	2.871
19	.9048	3.748	2.586	3.025
20	.9226	3.671	2.509	3.197
21	.9399	3.623	2.463	3.298
22	.9565	3.523	2.360	3.527
23	.9724	3.269	2.107	4.090

TABLE V

RING LOCATIONS & DIMENSIONS
RING STIFFENED CONE, CASE 3



RING NO.	r/r_b	h/r_b	ℓ/r_b	Δ/r_b
1	0.4321	1.117×10^{-3}	4.354×10^{-2}	0.991×10^{-3}
2	.5036	1.108	4.662	.306
3	.5629	1.107	4.885	0.
4	.6143	1.105	5.053	
5	.6595	1.088	5.077	
6	.7001	1.077	5.144	
7	.7370	1.066	5.176	
8	.7704	1.062	5.106	
9	.8002	1.031	4.980	
10	.8277	1.010	4.916	
11	.8535	.990	4.877	
12	.8778	.972	4.833	
13	.9010	.953	4.766	
14	.9229	.930	4.659	.075
15	.9436	.900	4.446	.313
16	.9627	.846	4.027	.788
				1.717

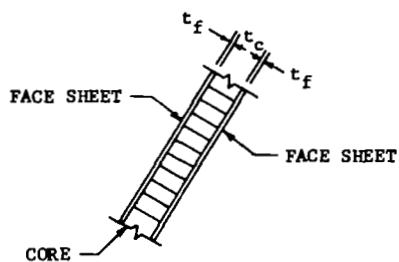
TABLE VI

RING LOCATIONS & DIMENSIONS
RING STIFFENED CONE, CASE 4

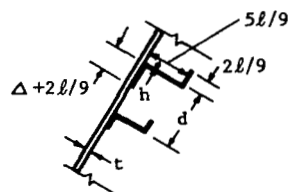
RING NO.	r/r_b	h/r_b	l/r_b	Δ/r_b
1	0.3723	1.085×10^{-4}	1.019×10^{-2}	2.121×10^{-3}
2	.4045	1.216	1.112	1.916
3	.4327	1.253	1.170	1.787
4	.4596	1.294	1.229	1.656
5	.4856	1.330	1.282	1.536
6	.5107	1.357	1.327	1.438
7	.5351	1.382	1.370	1.341
8	.5589	1.404	1.411	1.251
9	.5819	1.429	1.434	1.199
10	.6037	1.444	1.446	1.172
11	.6245	1.457	1.456	1.151
12	.6444	1.467	1.462	1.138
13	.6634	1.476	1.466	1.129
14	.6818	1.482	1.470	1.119
15	.6996	1.488	1.476	1.106
16	.7168	1.490	1.477	1.103
17	.7336	1.491	1.476	1.105
18	.7499	1.491	1.474	1.111
19	.7658	1.489	1.469	1.121
20	.7812	1.484	1.461	1.140
21	.7963	1.478	1.450	1.163
22	.8110	1.470	1.438	1.191
23	.8253	1.460	1.421	1.227
24	.8393	1.447	1.403	1.268
25	.8530	1.431	1.384	1.311
26	.8664	1.414	1.362	1.360
27	.8795	1.394	1.337	1.416
28	.8923	1.371	1.307	1.482
29	.9048	1.342	1.271	1.562
30	.9171	1.307	1.226	1.661
31	.9290	1.262	1.171	1.785
32	.9407	1.205	1.101	1.939
33	.9520	1.132	1.015	2.130
34	.9629	1.037	.909	2.367
35	.9734	.910	.774	2.667
36	.9835	.877	.578	3.103

TABLE VII
RING LOCATIONS & DIMENSIONS
RING STIFFENED CONE, CASE 5

RING NO.	r/r_b	h/r_b	l/r_b	Δ/r_b
1	0.3805	3.404×10^{-4}	1.793×10^{-2}	0.786×10^{-3}
2	.4217	3.722	1.969	.396
3	.4549	3.688	2.031	.258
4	.4856	3.745	2.116	.070
5	.5143	3.795	2.189	0.
6	.5414	3.821	2.240	
7	.5671	3.856	2.299	
8	.5915	3.889	2.353	
9	.6149	3.894	2.383	
10	.6372	3.900	2.413	
11	.6585	3.899	2.435	
12	.6790	3.916	2.447	
13	.6982	3.915	2.443	
14	.7164	3.907	2.436	
15	.7336	3.895	2.434	
16	.7503	3.863	2.444	
17	.7666	3.837	2.452	
18	.7825	3.819	2.463	
19	.7981	3.796	2.463	
20	.8132	3.763	2.454	
21	.8279	3.728	2.442	
22	.8423	3.689	2.425	
23	.8562	3.648	2.405	
24	.8698	3.605	2.382	
25	.8830	3.559	2.355	
26	.8959	3.509	2.322	
27	.9084	3.454	2.278	
28	.9206	3.385	2.219	
29	.9323	3.298	2.139	.020
30	.9436	3.184	2.031	.259
31	.9544	3.034	1.886	.580
32	.9646	2.835	1.701	.756
33	.9742	2.575	1.464	1.133
34	.9830	2.282	1.174	1.778
35	.9908	1.932	.898	2.390

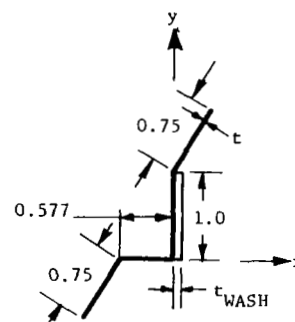
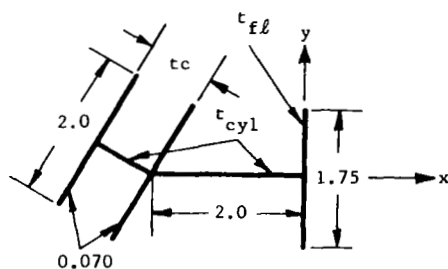
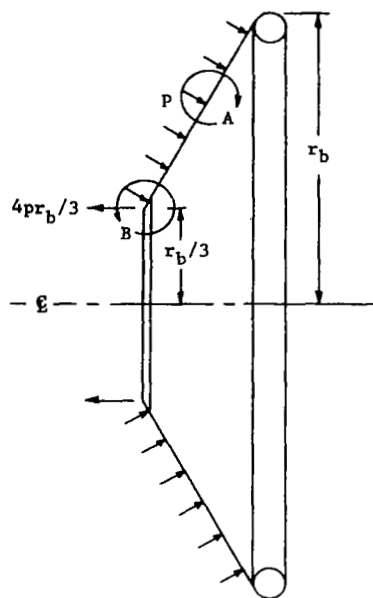


SANDWICH SHELLS



RING-STIFFENED SHELLS

DETAIL A, WALL SECTIONS



r_b	$p/E \times 10^7$	t_{cyl}	t_{fl}
57	2	0.050	0.050
	10	.070	.050
	50	.119	.090
114	2	.052	.050
	10	.088	.057
	50	.150	.127

SANDWICH SHELLS

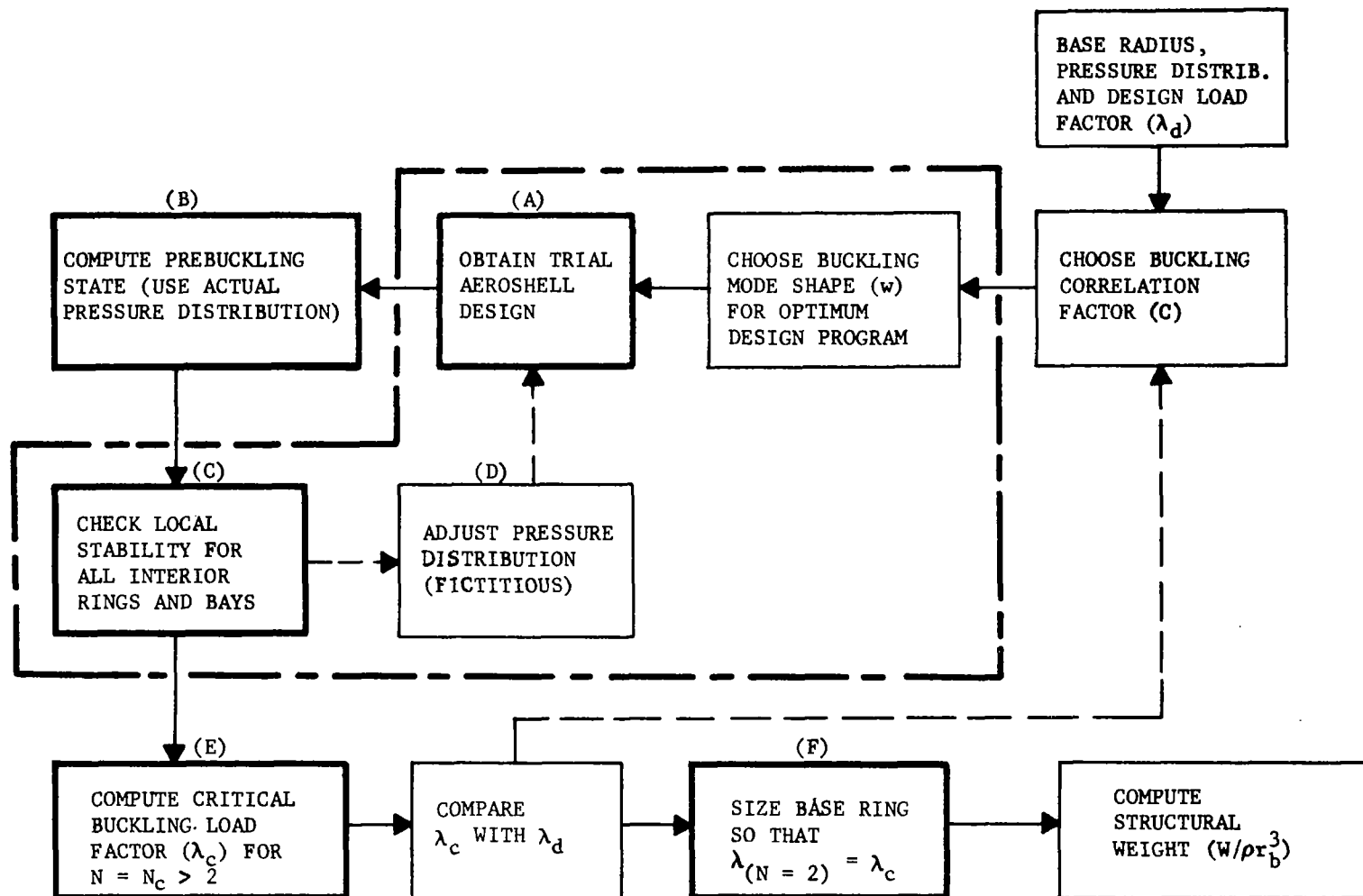
r_b	$p/E \times 10^7$	t	t_{wash}
57	2	0.040	---
	10	.090	---
	50	.100	0.175
114	2	0.060	---
	10	.125	---
	50	.125	0.250

RING-STIFFENED SHELLS

DETAIL B, NOSE RINGS

FIGURE 1. SHELL CONFIGURATIONS TREATED

FIGURE 2. OPTIMUM DESIGN FLOW CHART



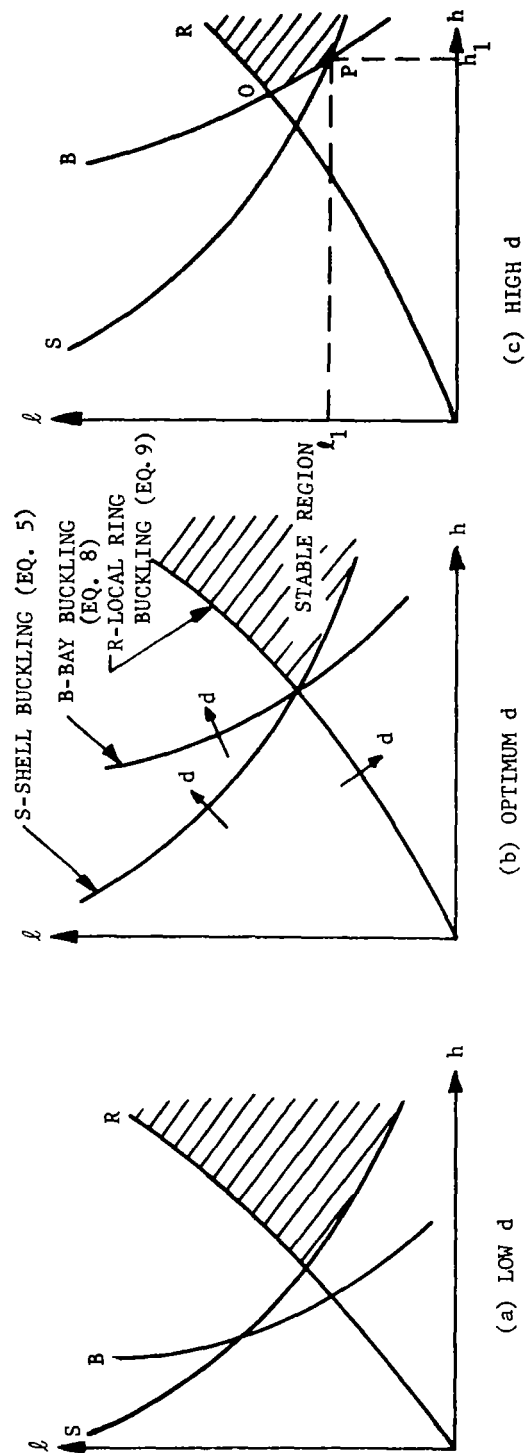


FIGURE 3. SCHEMATIC SOLUTION FOR OPTIMUM RING SIZE AND SPACING (NEGLECTING CONSTRAINTS), hl/d IS MINIMIZED AT COMMON INTERSECTION

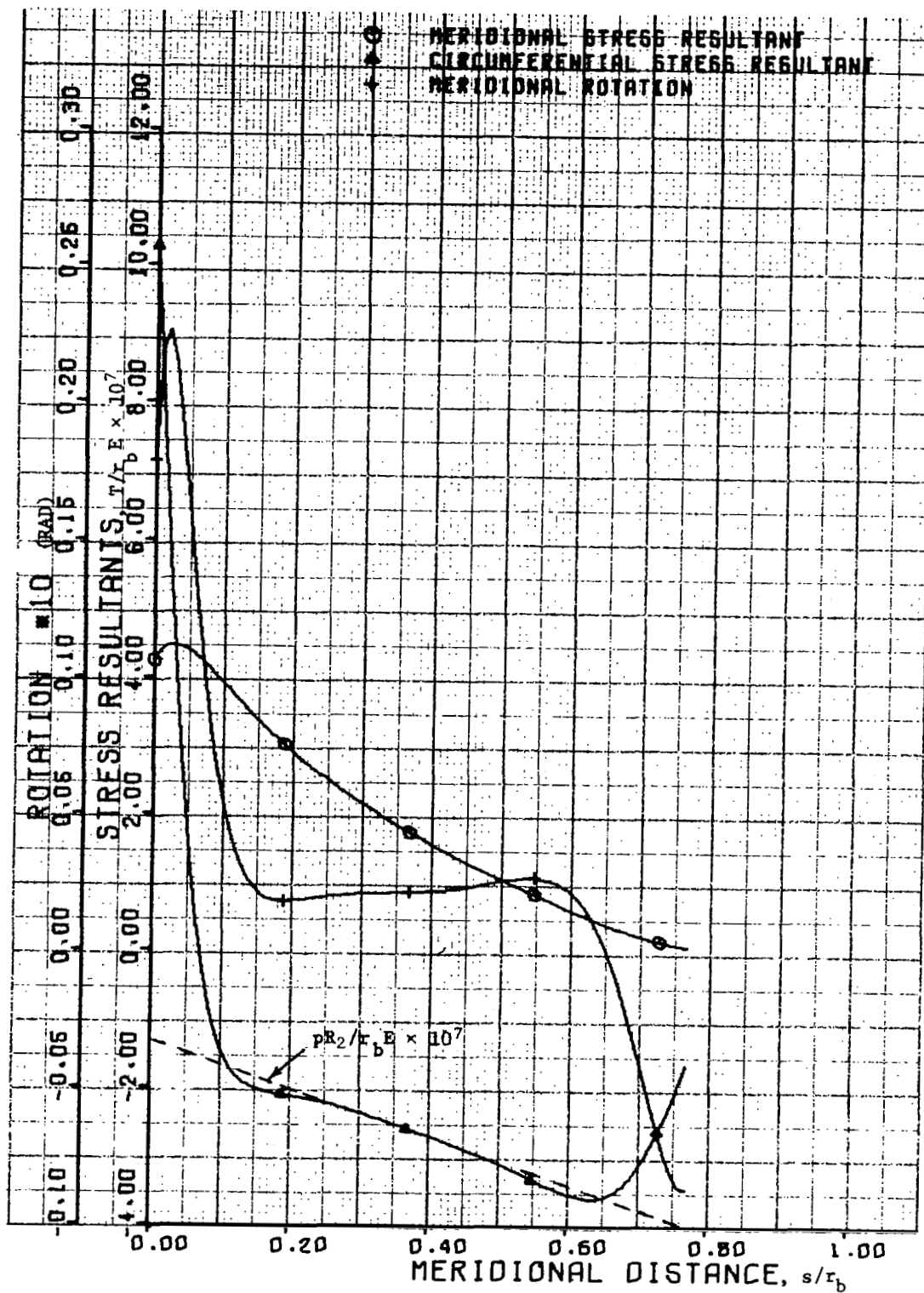


FIGURE 4. PREBUCKLING STRESS RESULTANTS AND ROTATION
 SANDWICH CONE ($p/E = 2.00 \times 10^{-7}$, $r_b = 57$ IN.)

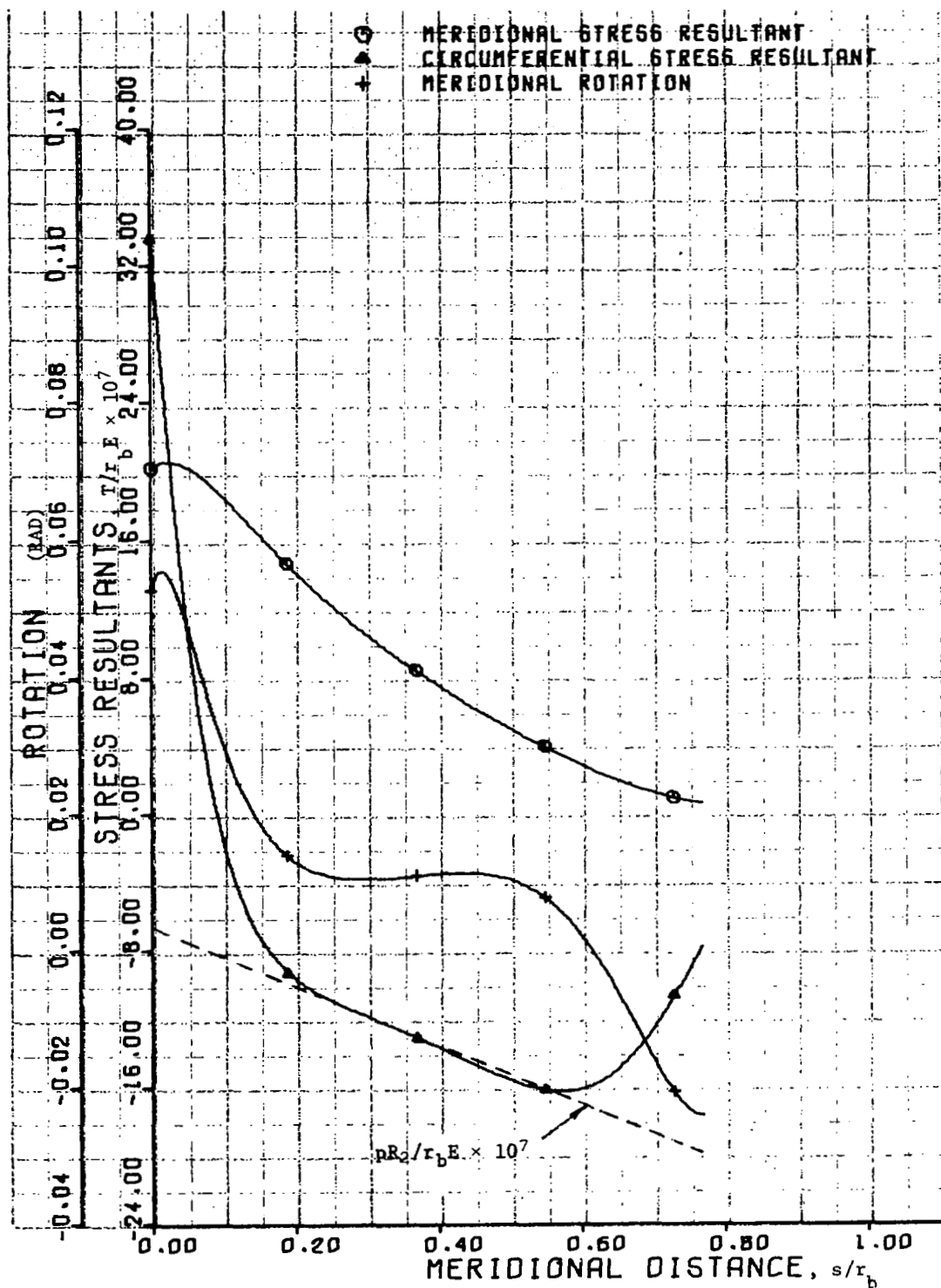


FIGURE 5. PREBUCKLING STRESS RESULTANTS AND ROTATION
 SANDWICH CONE ($p/E = 9.88 \times 10^{-7}$, $r_b = 57$ IN.)

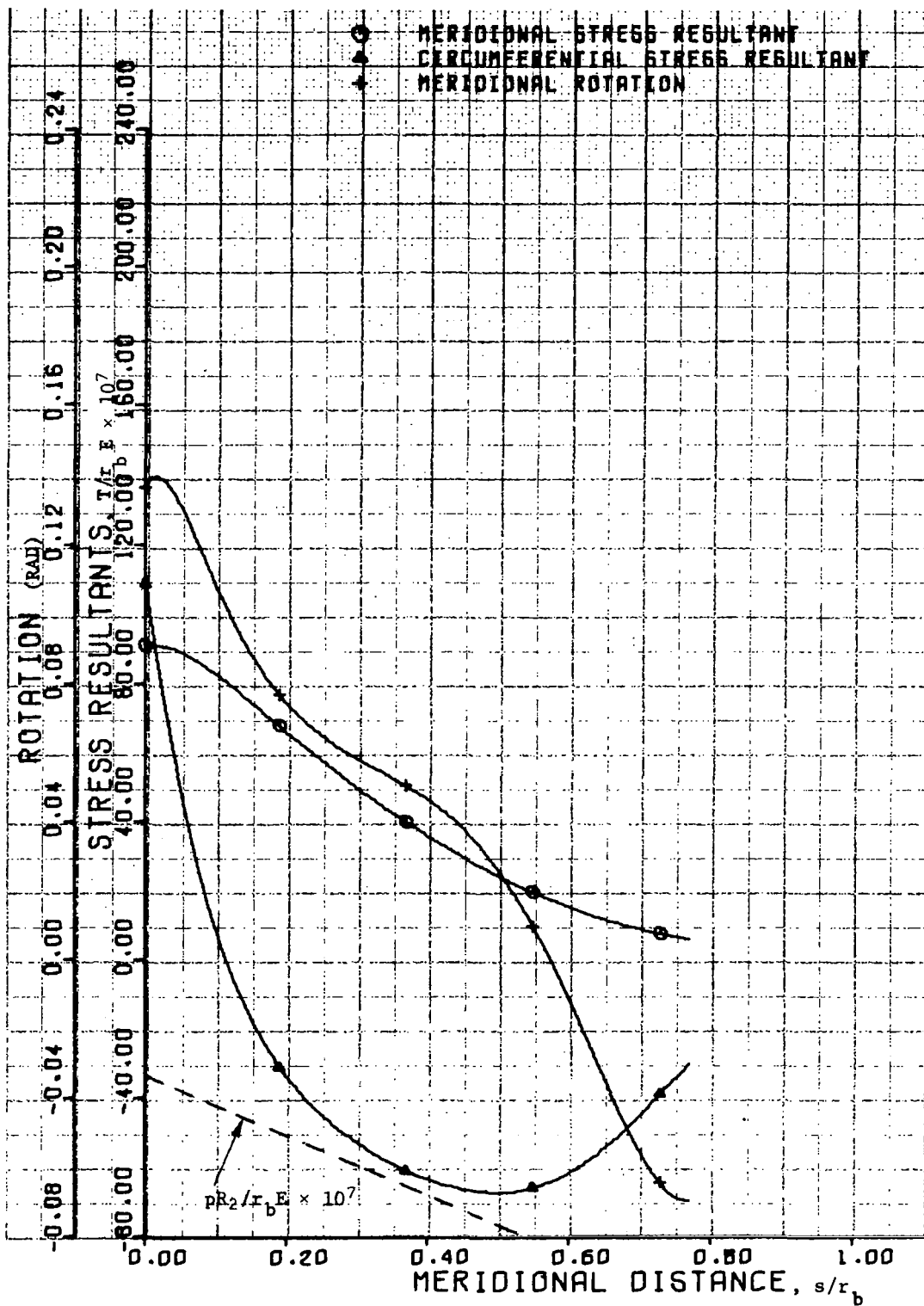


FIGURE 6. PREBUCKLING STRESS RESULTANTS AND ROTATION
 SANDWICH CONE ($p/E = 50.33 \times 10^{-7}$, $r_b = 57$ IN.)

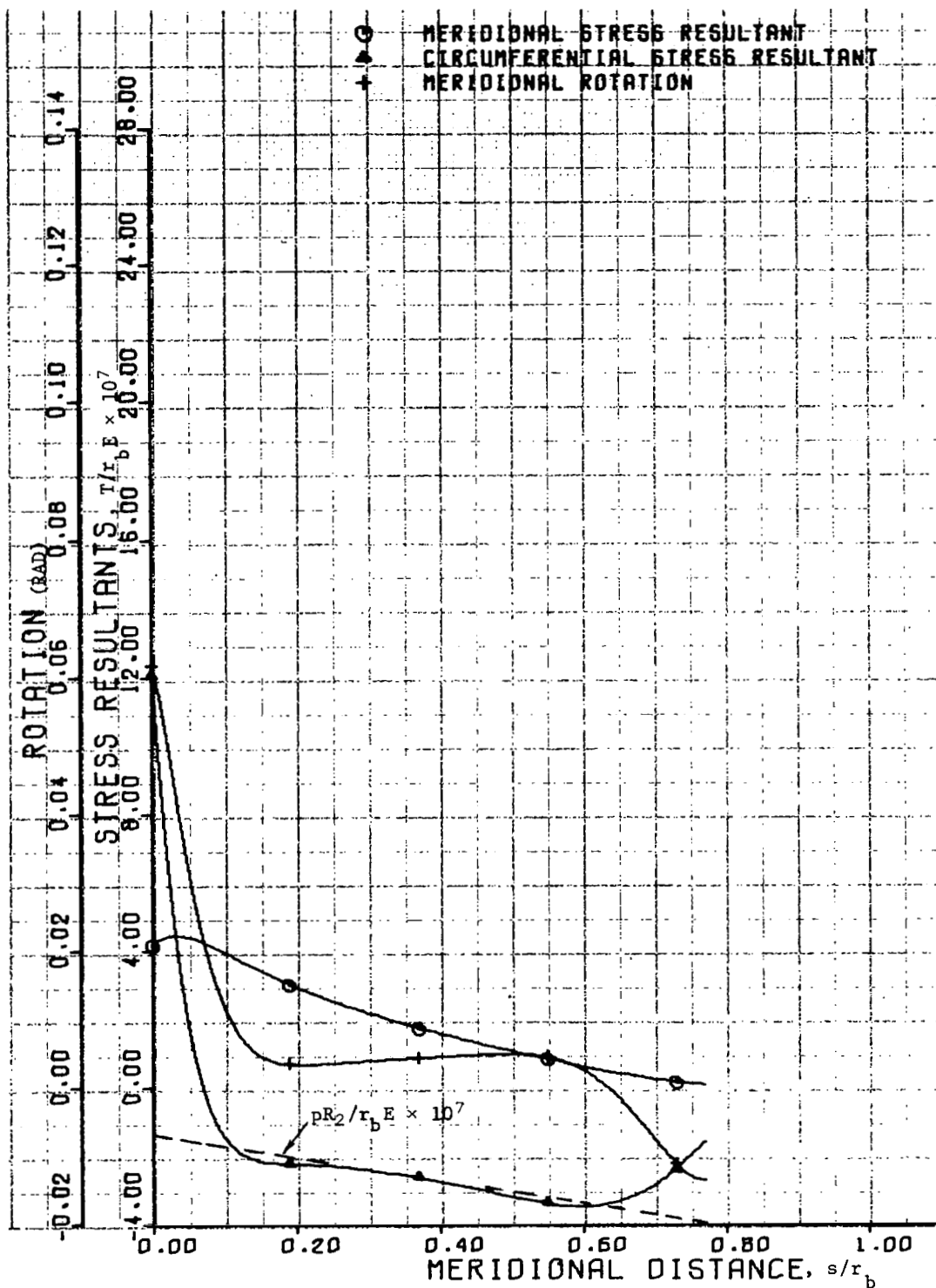


FIGURE 7. PREBUCKLING STRESS RESULTANTS AND ROTATION
SANDWICH CONE ($p/E = 2.00 \times 10^{-7}$, $r_b = 114$ IN.)

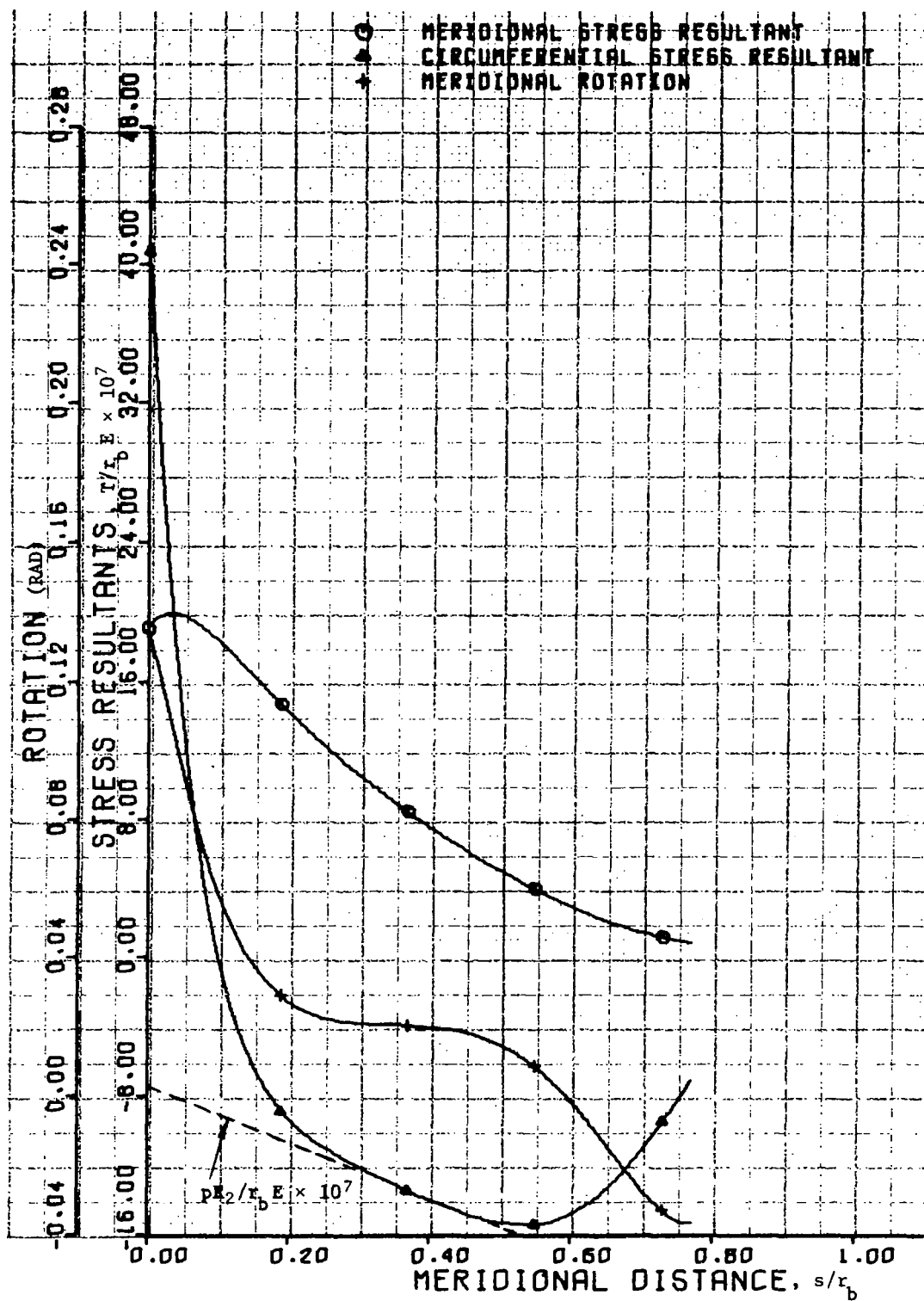


FIGURE 8. PREBUCKLING STRESS RESULTANTS AND ROTATION
 SANDWICH CONE ($p/E = 10.03 \times 10^{-7}$, $r_b = 114$ IN.)

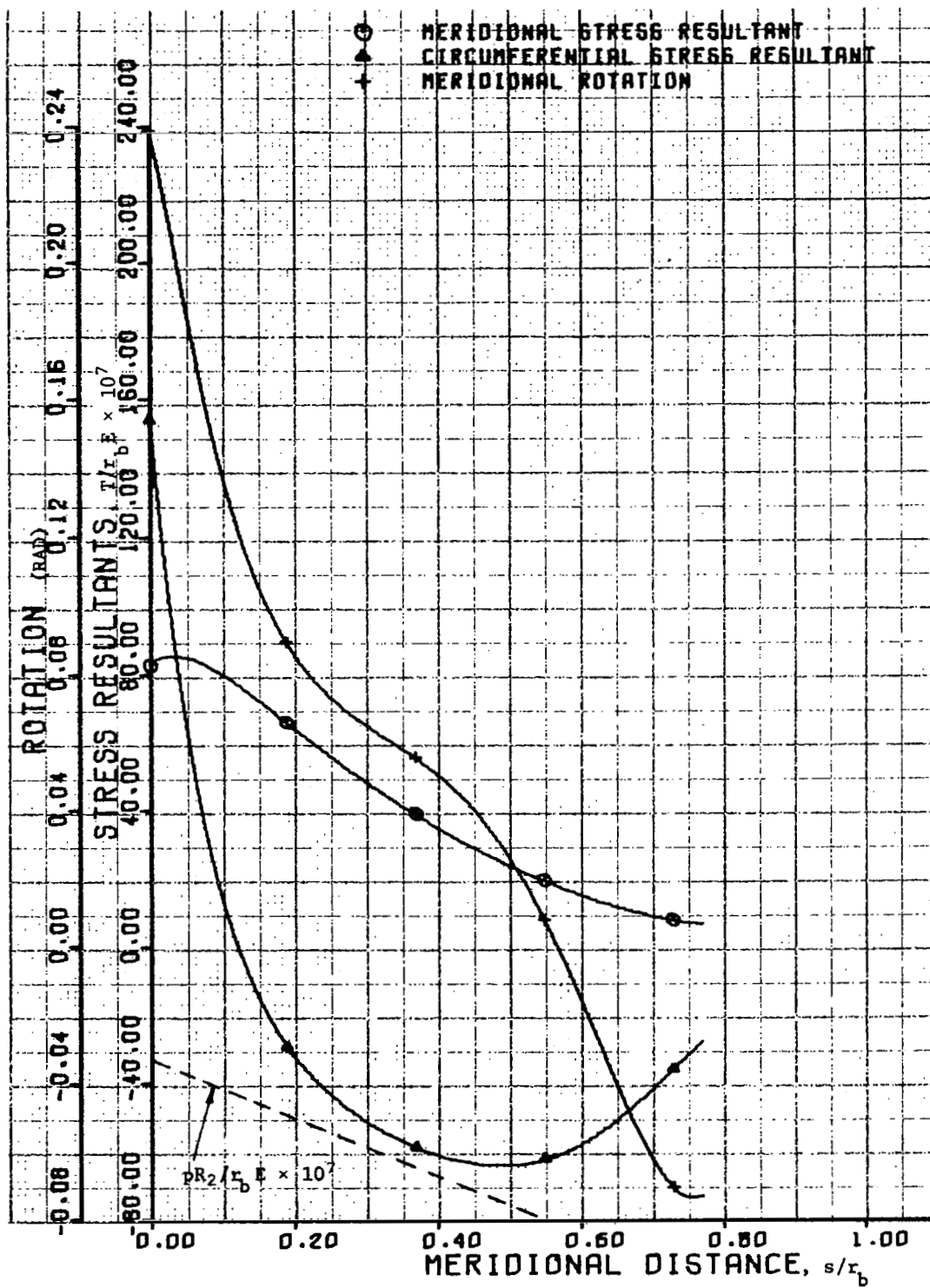


FIGURE 9. PREBUCKLING STRESS RESULTANTS AND ROTATION
SANDWICH CONE ($p/E = 49.57 \times 10^{-7}$, $r_b = 114$ IN.)

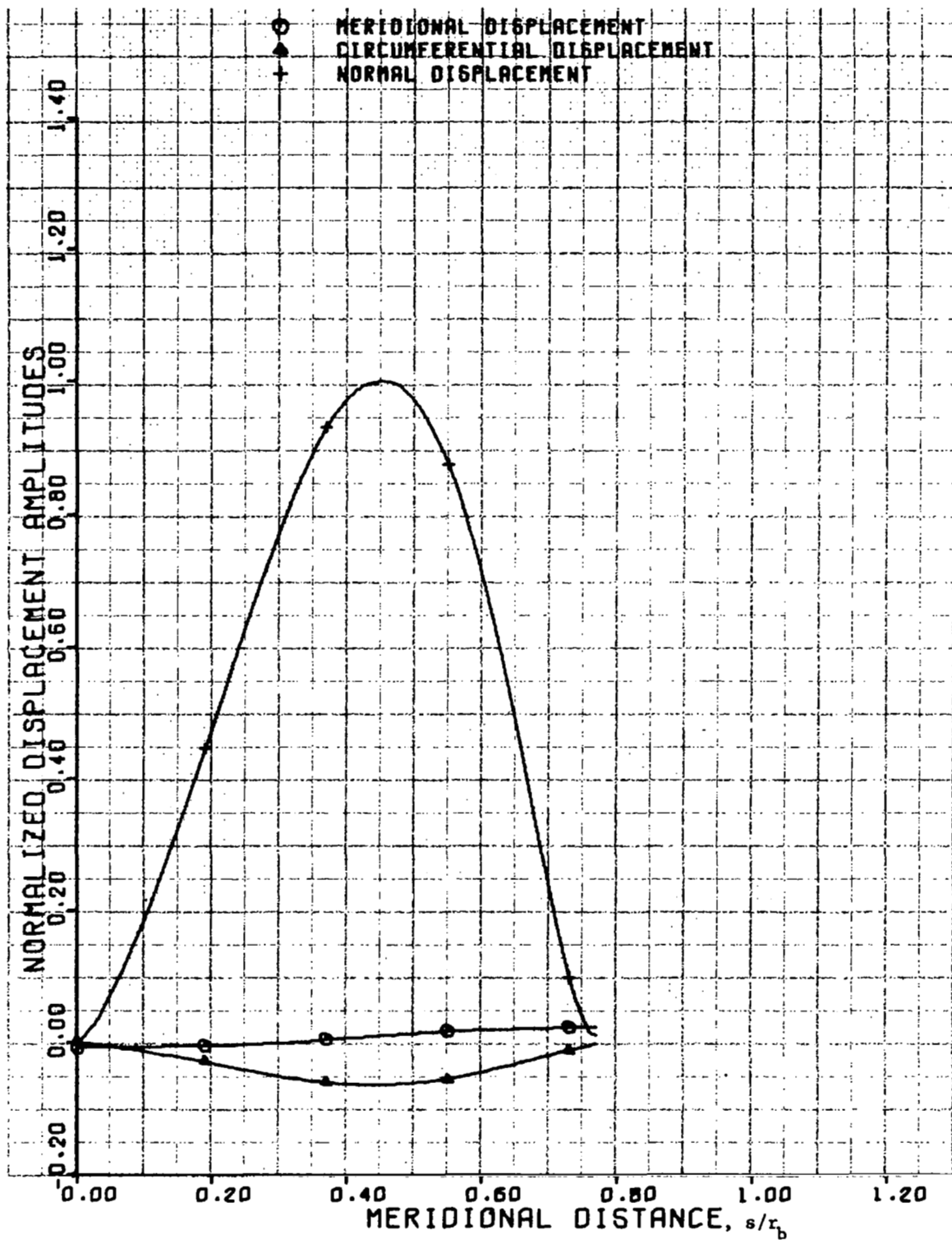


FIGURE 10. BUCKLING MODE DISPLACEMENTS
SANDWICH CONE ($p/E = 2.00 \times 10^{-7}$, $r_b = 57$ IN.) $N = 8$

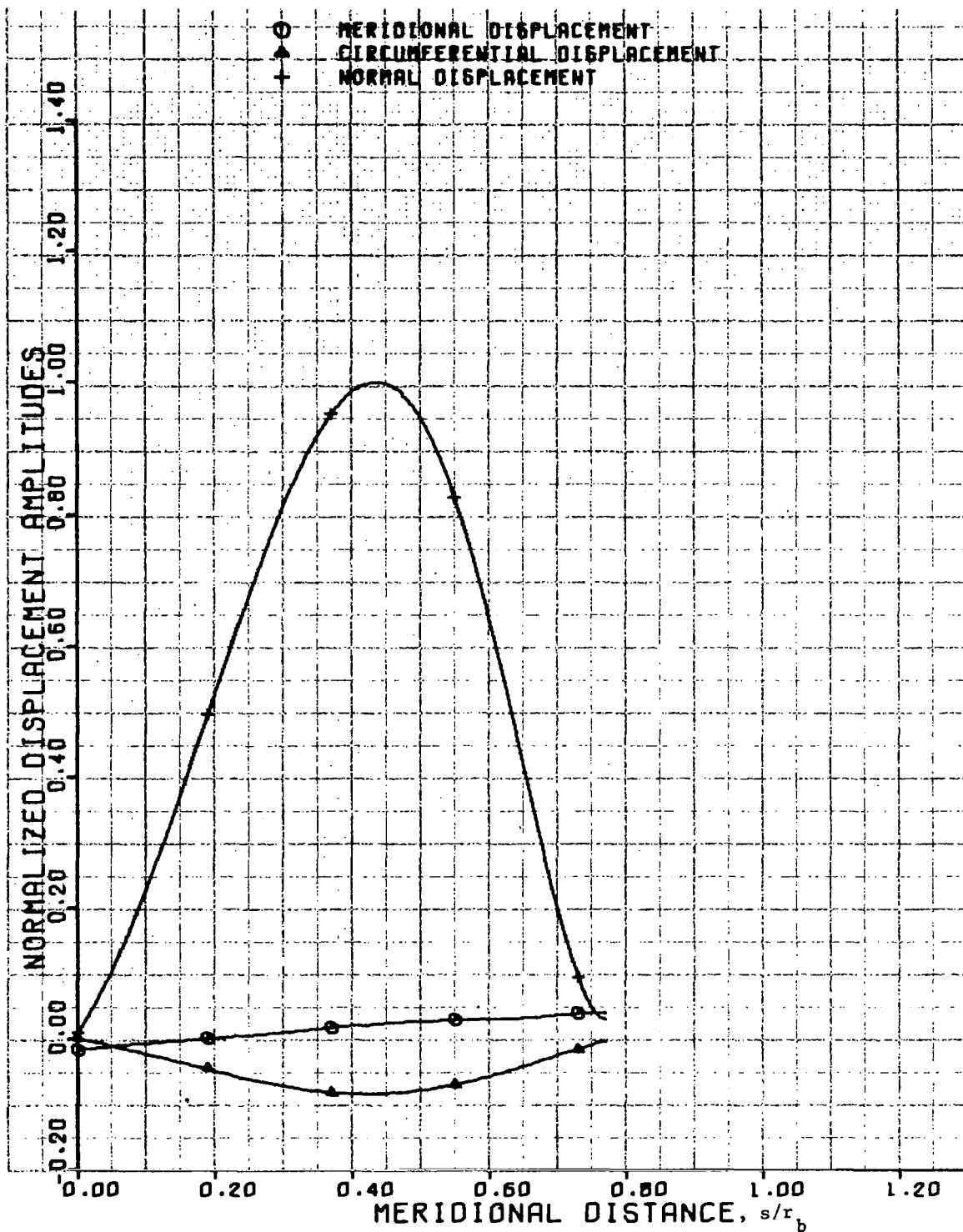


FIGURE 11. BUCKLING MODE DISPLACEMENTS
 SANDWICH CONE ($p/E = 9.88 \times 10^{-7}$, $r_b = 57$ IN.) $N = 6$

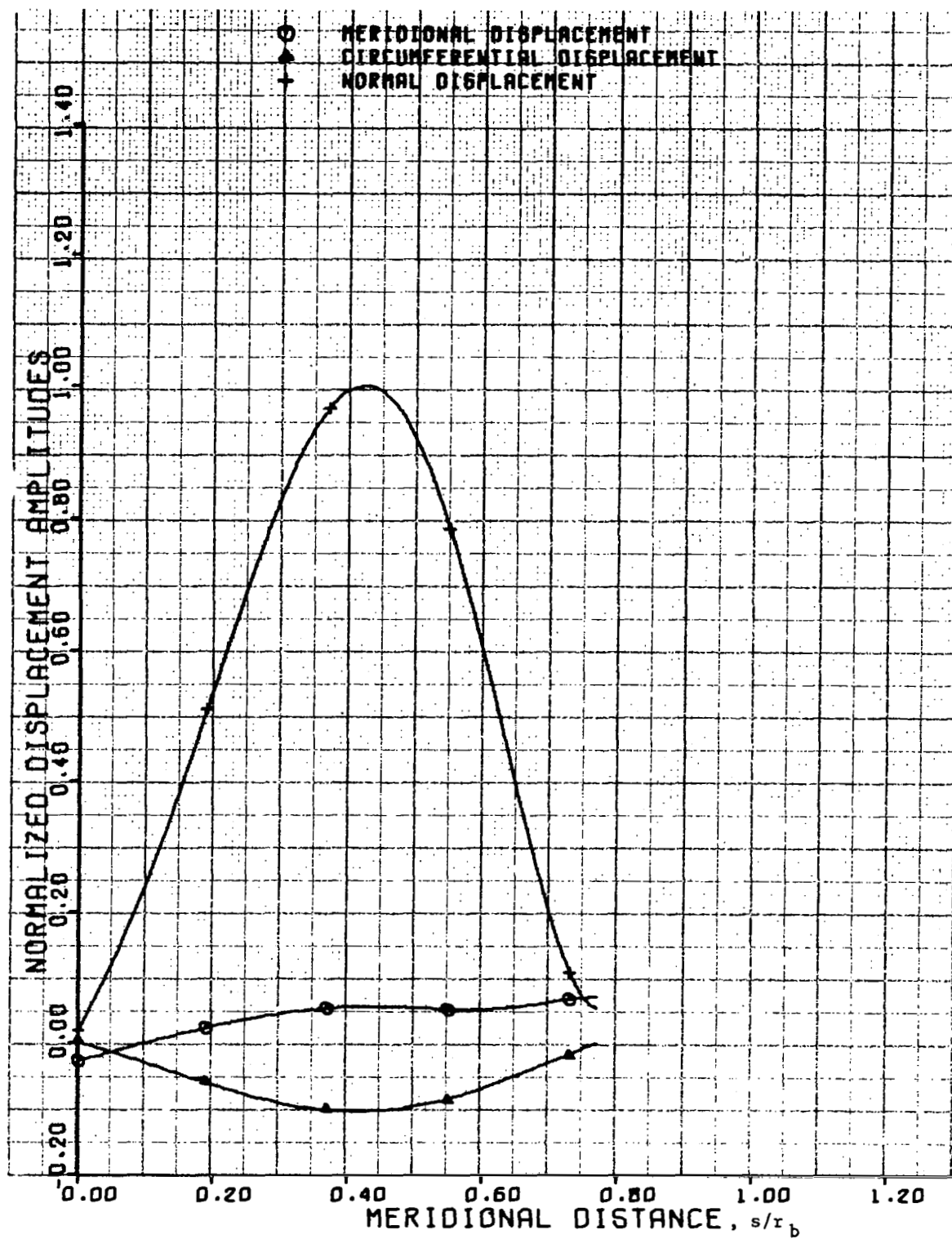


FIGURE 12. BUCKLING MODE DISPLACEMENTS
 SANDWICH CONE ($p/E = 50.33 \times 10^{-7}$, $r_b = 57$ IN.) $N = 5$

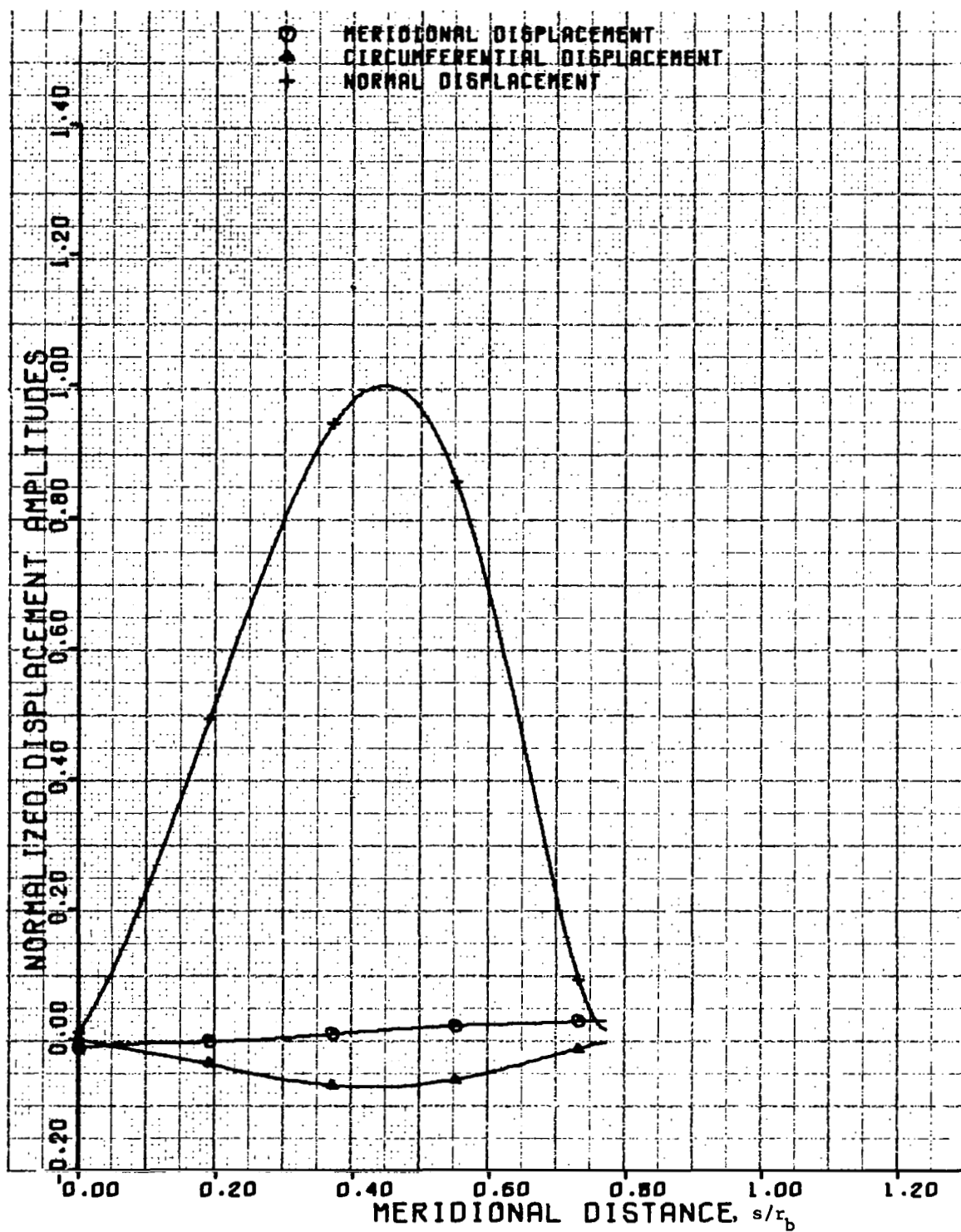


FIGURE 13. BUCKLING MODE DISPLACEMENTS
 SANDWICH CONE ($p/E = 2.00 \times 10^{-7}$, $r_b = 114$ IN.) $N = 7$

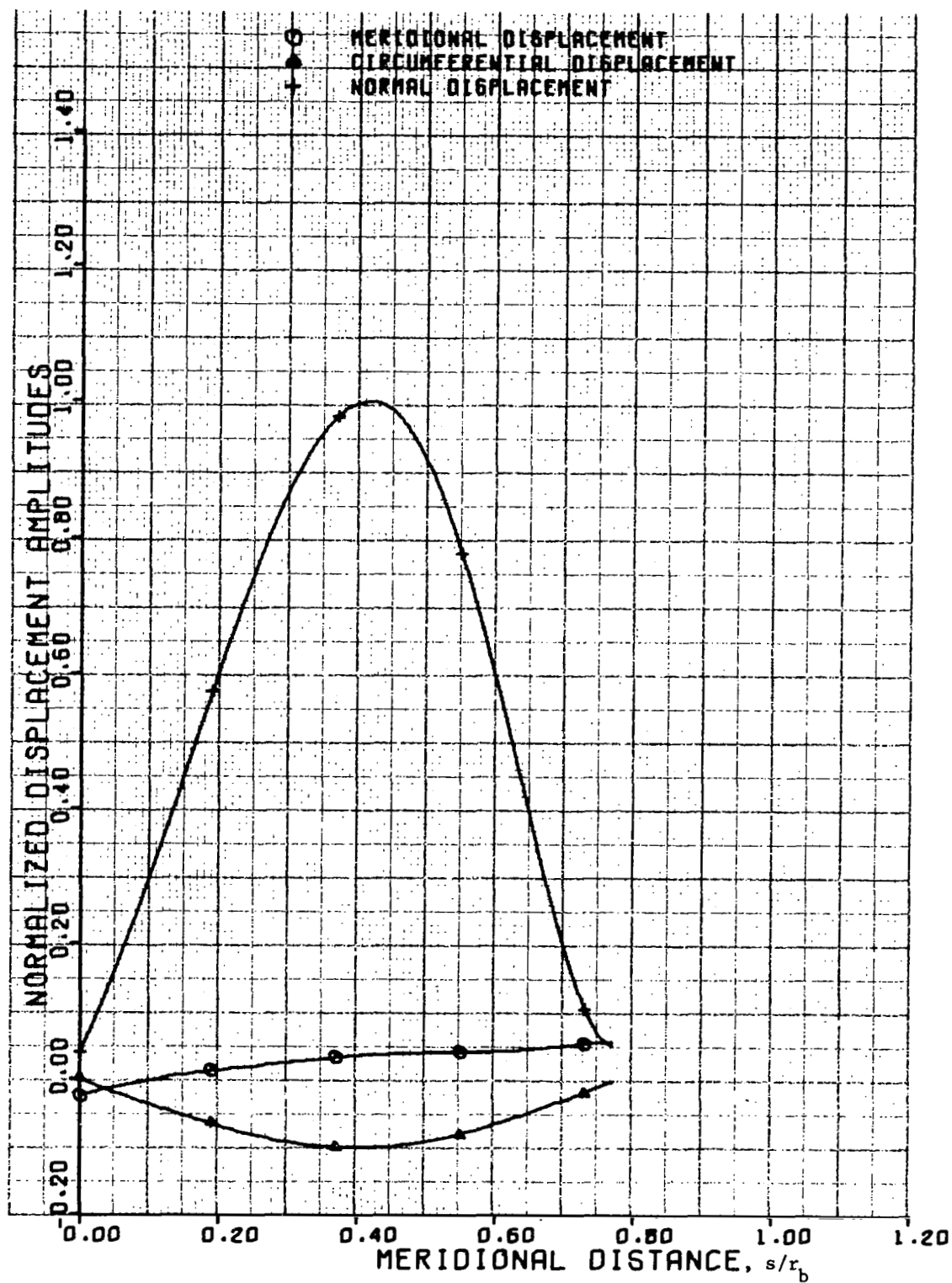


FIGURE 14. BUCKLING MODE DISPLACEMENTS
 SANDWICH CONE ($p/E = 10.03 \times 10^{-7}$, $r_b = 114$ IN.) $N = 5$

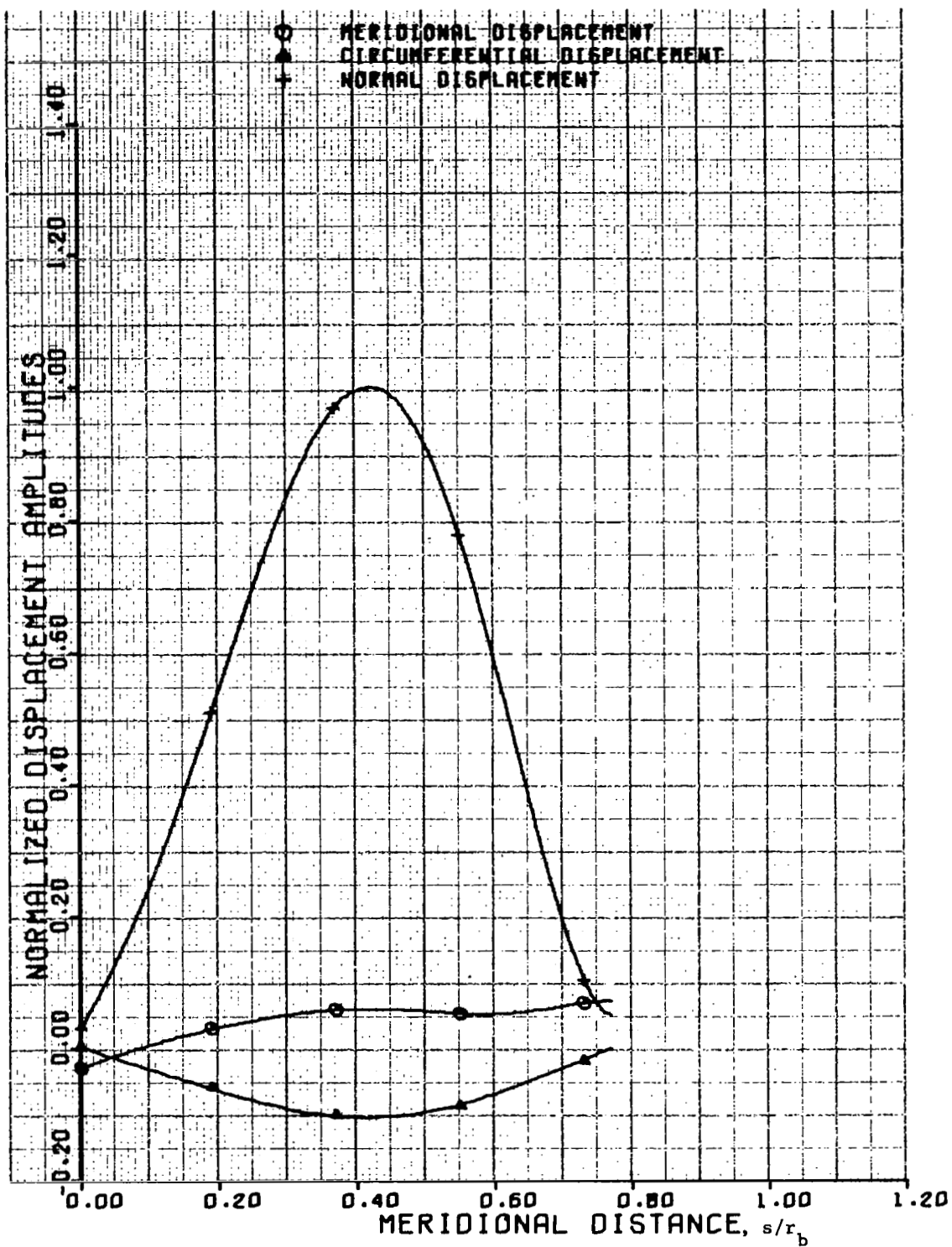


FIGURE 15. BUCKLING MODE DISPLACEMENTS
SANDWICH CONE ($p/E = 49.57 \times 10^{-7}$, $r_b = 114$ IN.) $N = 5$

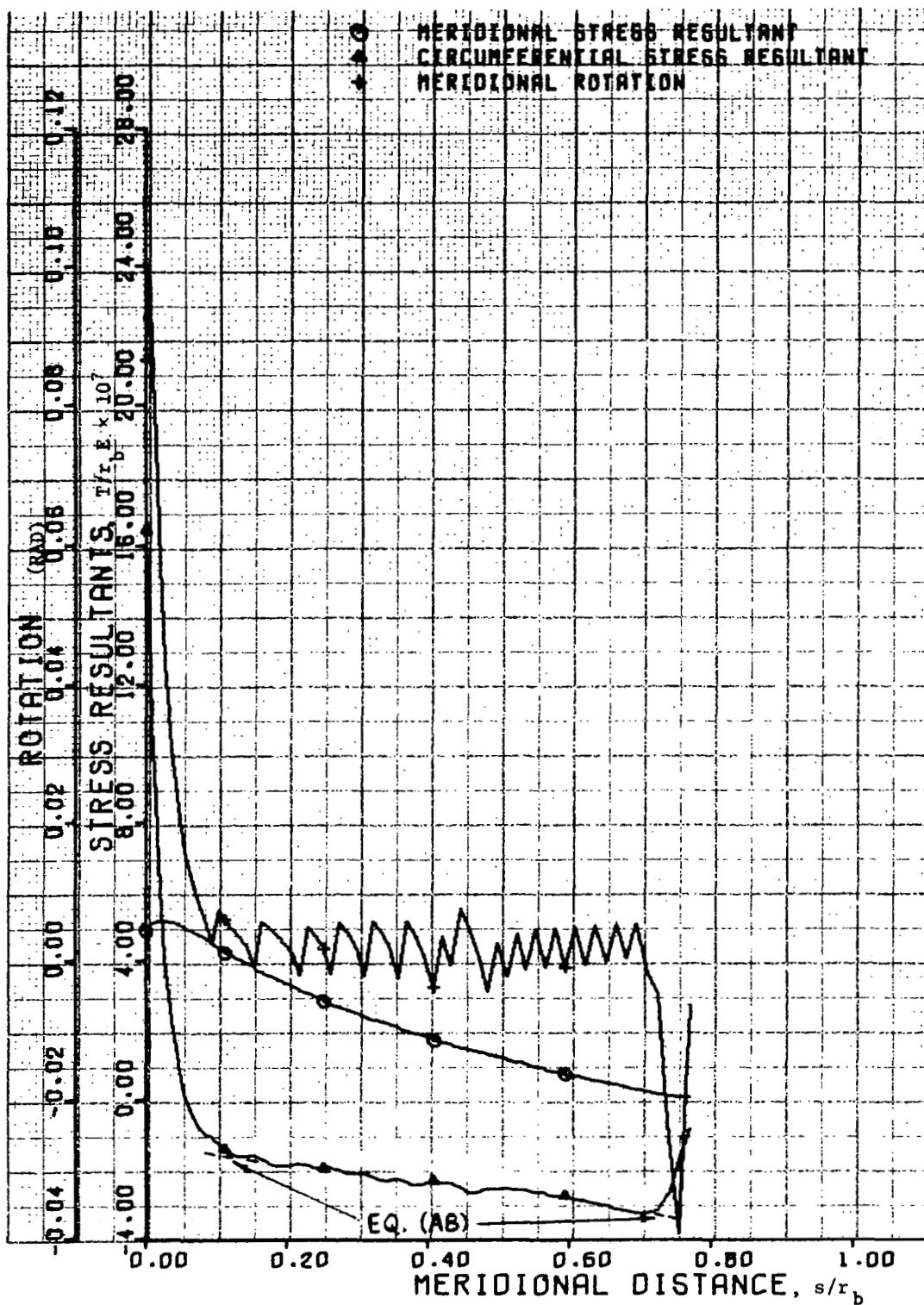


FIGURE 16. PREBUCKLING STRESS RESULTANTS AND ROTATION
RING-STIFFENED CONE ($p/E = 2.27 \times 10^{-7}$, $r_b = 57$ IN.)

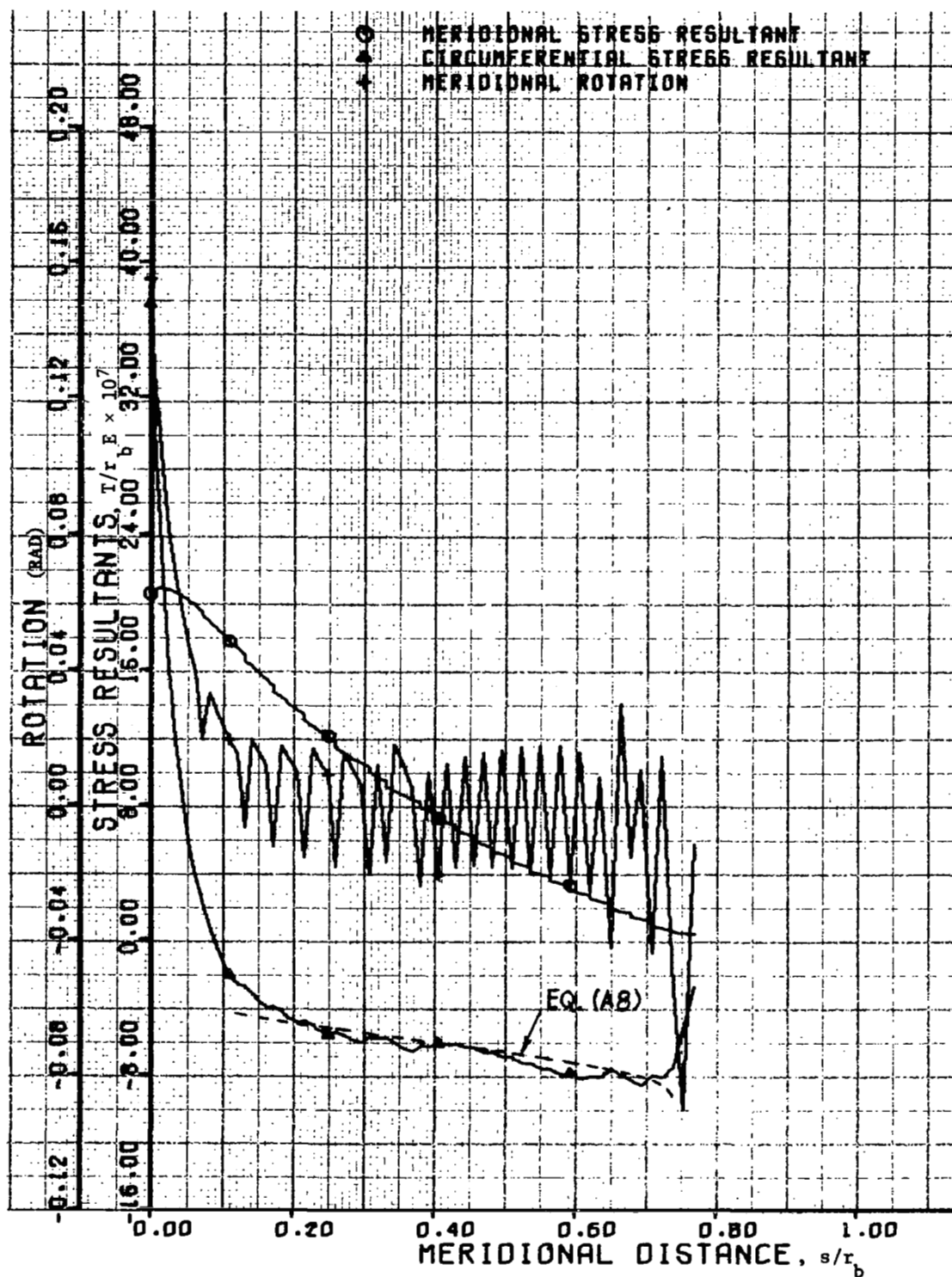


FIGURE 17. PREBUCKLING STRESS RESULTANTS AND ROTATION
 RING-STIFFENED CONE ($p/E = 9.69 \times 10^{-7}$, $r_b = 57$ IN.)

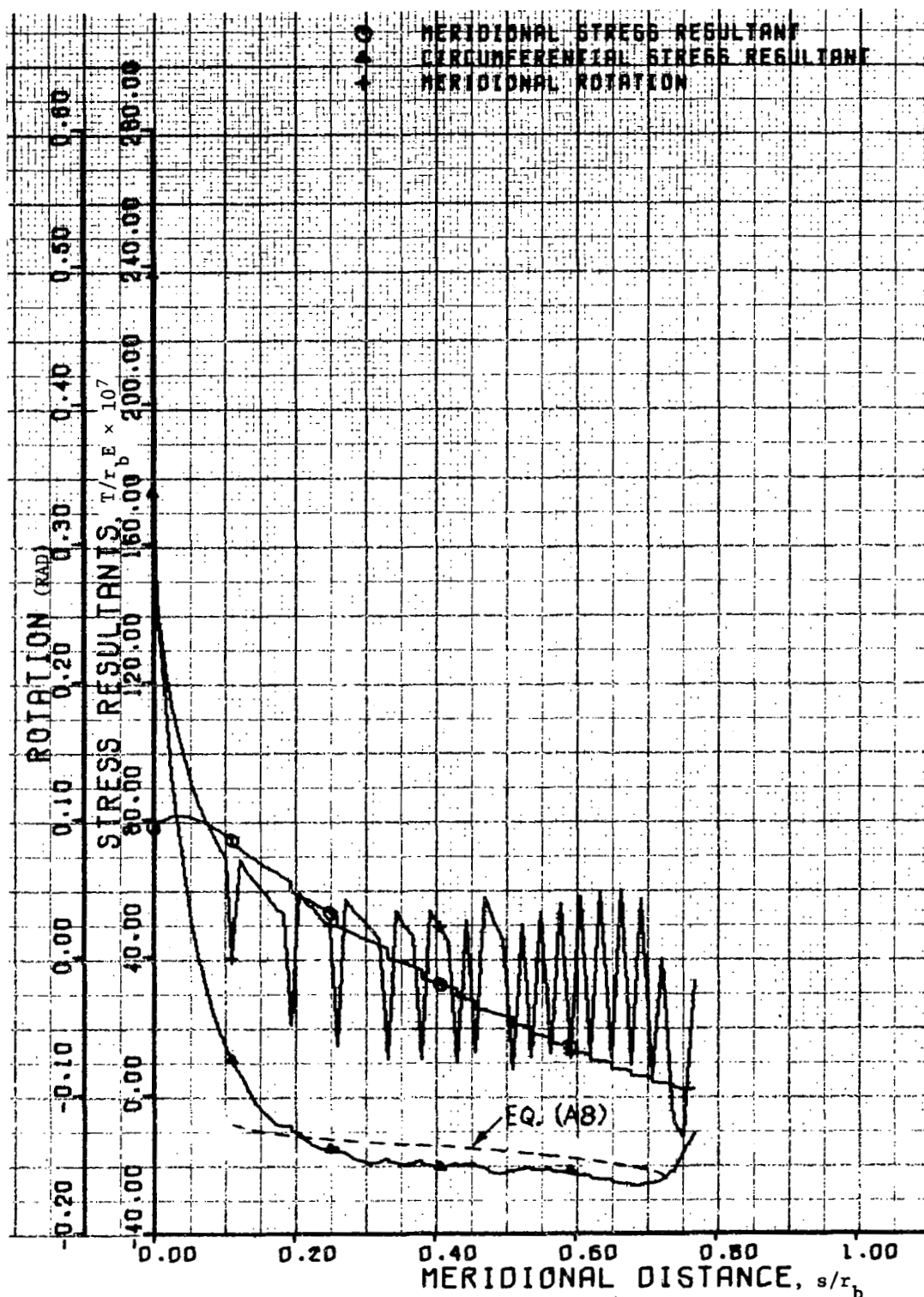


FIGURE 18. PREBUCKLING STRESS RESULTANTS AND ROTATION
 RING-STIFFENED CONE ($p/E = 43.15 \times 10^{-7}$, $r_b \approx 57$ IN.)

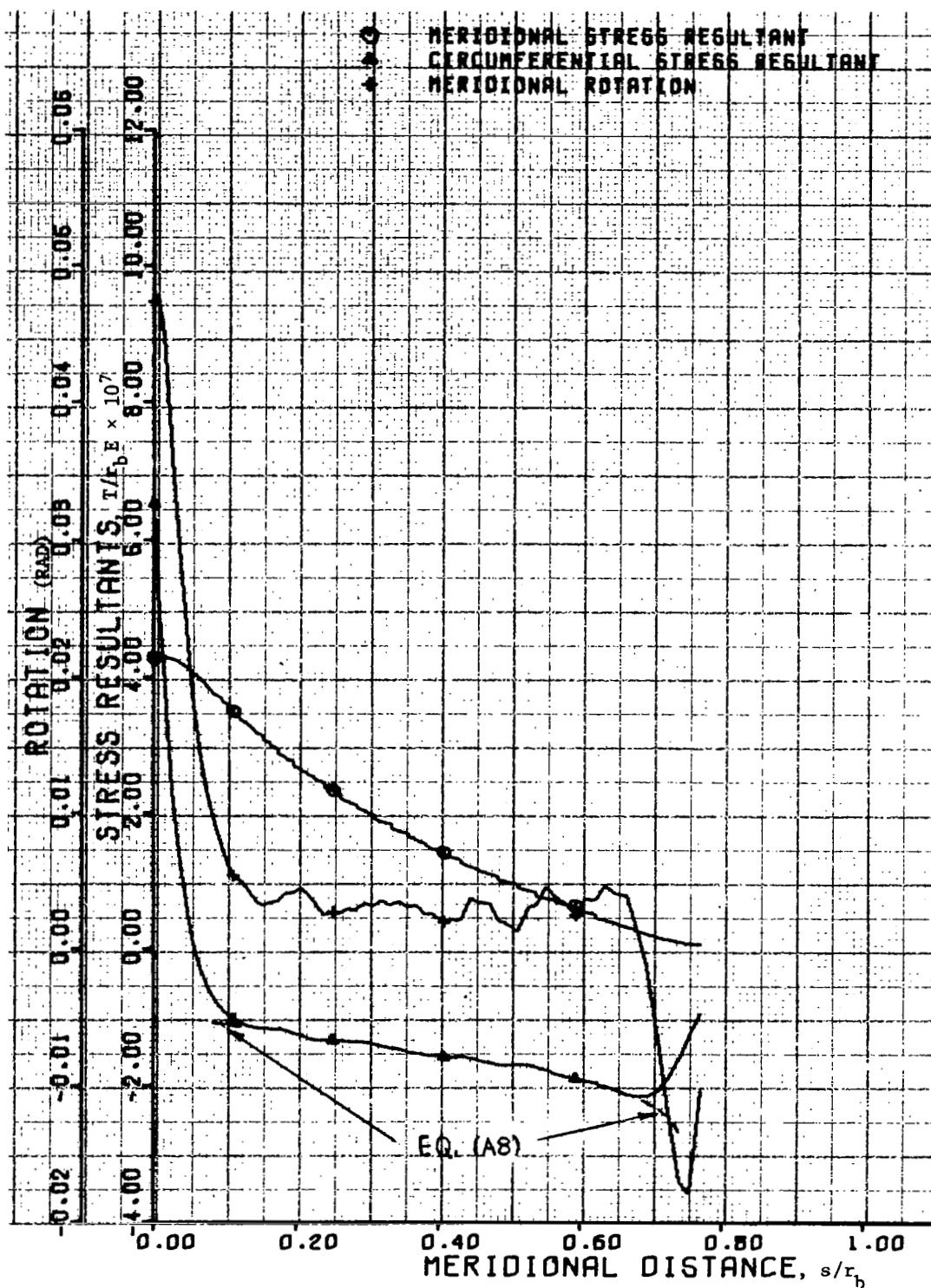


FIGURE 19. PREBUCKLING STRESS RESULTANTS AND ROTATION
 RING-STIFFENED CONE ($p/E = 1.86 \times 10^{-7}$, $r_b = 114$ IN.)

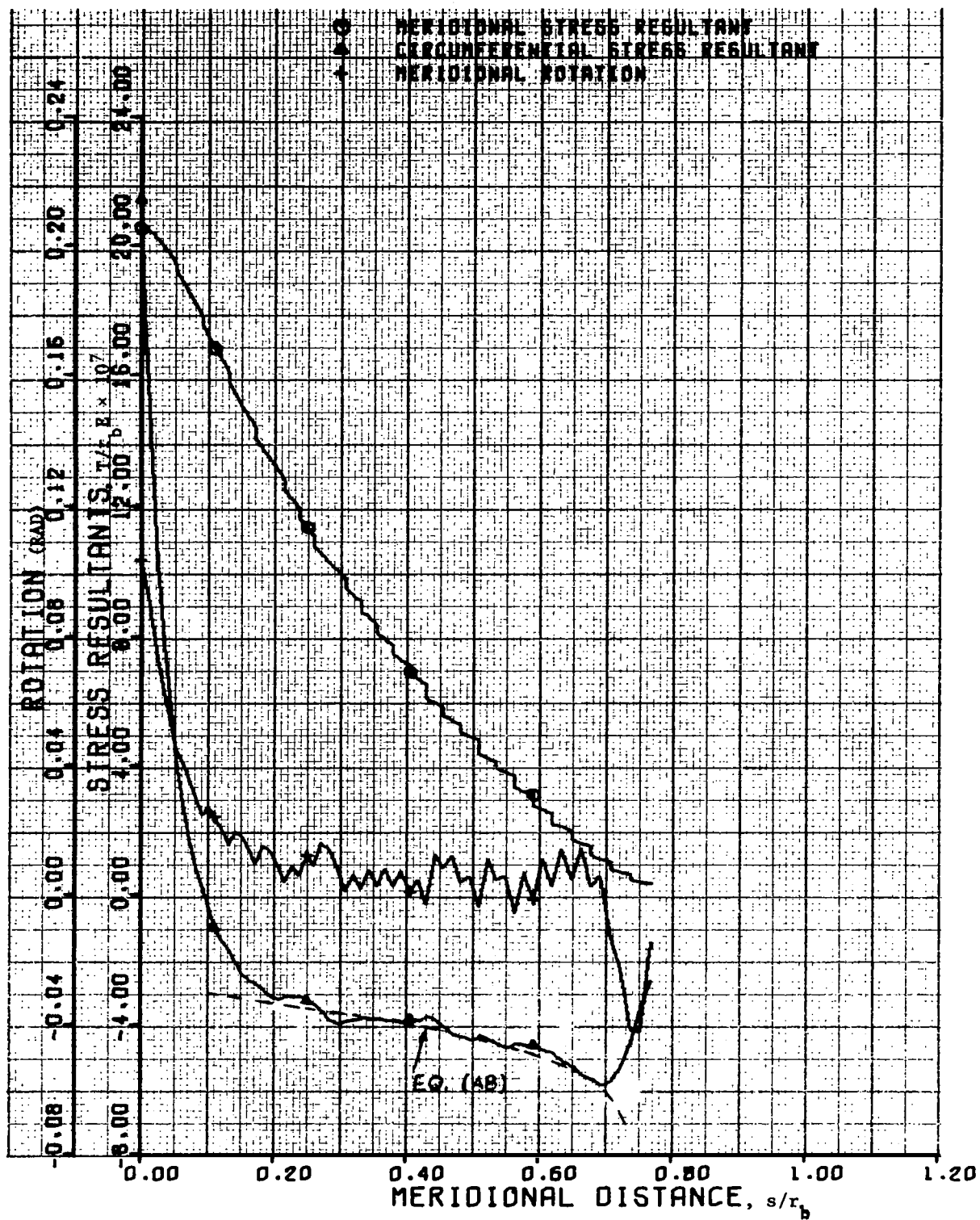


FIGURE 20. PREBUCKLING STRESS RESULTANTS AND ROTATION
 RING-STIFFENED CONE ($p/E = 9.28 \times 10^{-7}$, $r_b = 114$ IN.)

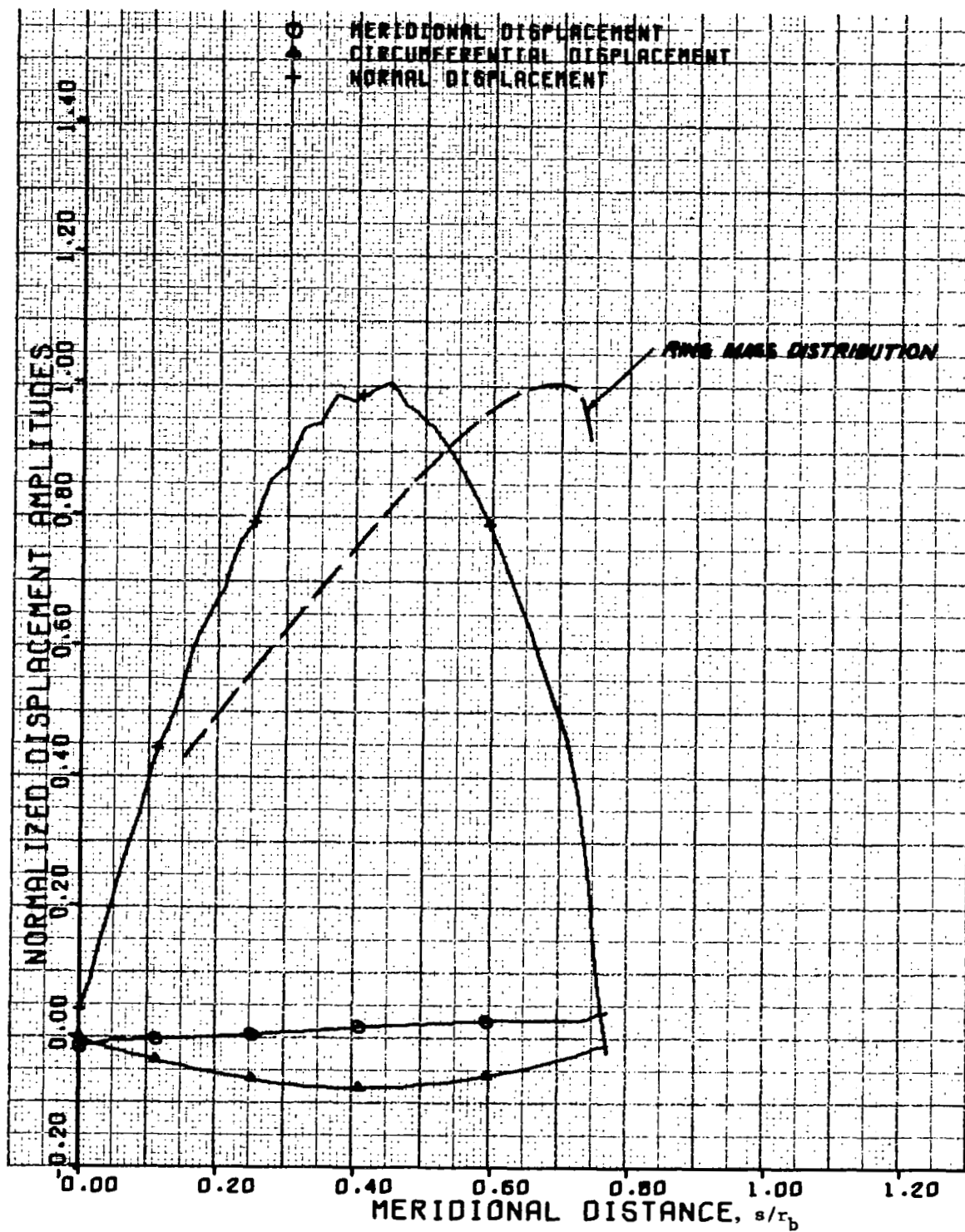


FIGURE 21. BUCKLING MODE DISPLACEMENTS
 RING-STIFFENED CONE ($p/E = 2.27 \times 10^{-7}$, $r_b = 57$ IN.) $N = 6$

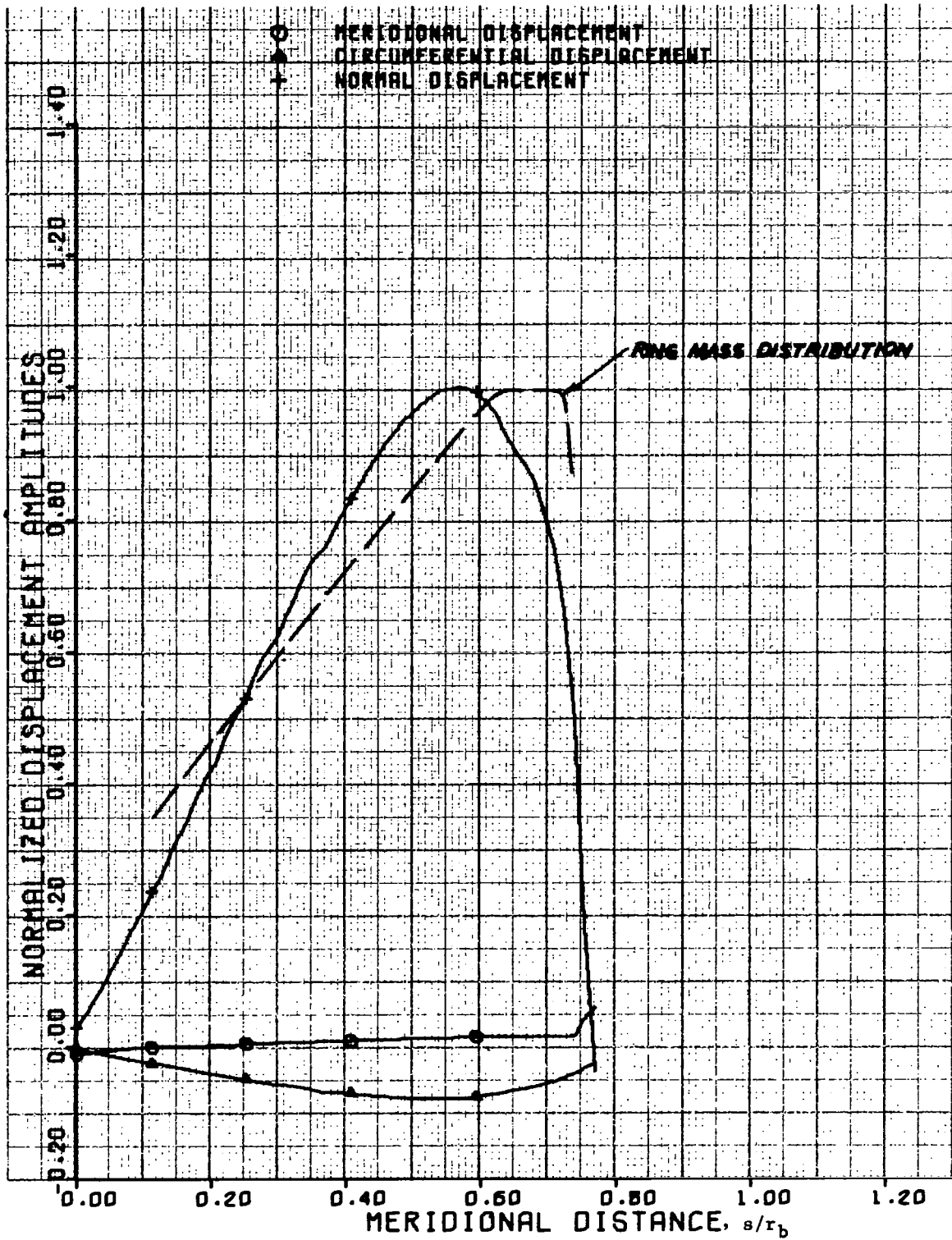


FIGURE 22. BUCKLING MODE DISPLACEMENTS
RING-STIFFENED CONE ($p/E = 9.69 \times 10^{-7}$, $r_b = 57$ IN.) $N = 5$

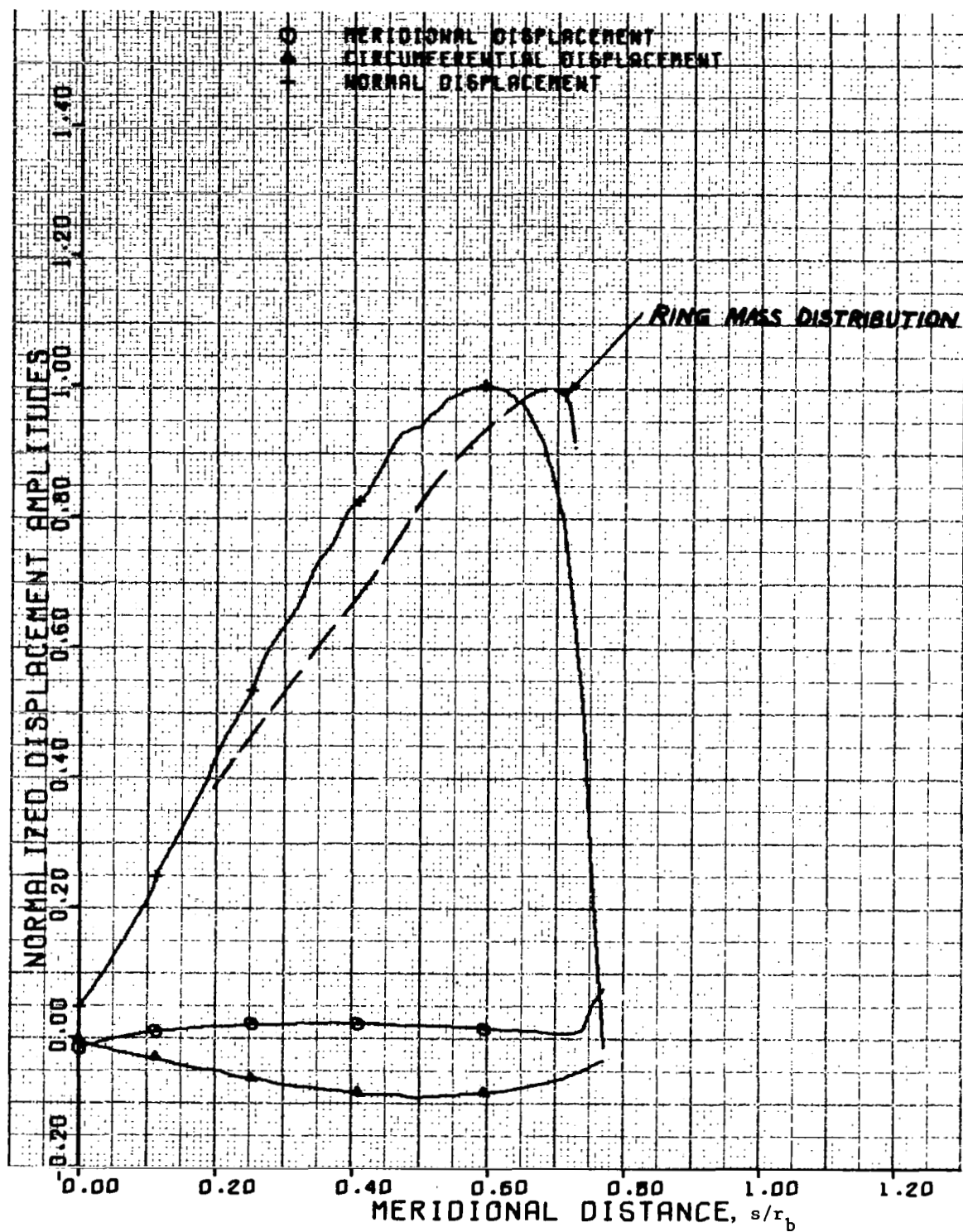


FIGURE 23. BUCKLING MODE DISPLACEMENTS
RING-STIFFENED CONE ($p/E = 43.15 \times 10^{-7}$, $r_b \geq 57$ IN.) $N = 4$

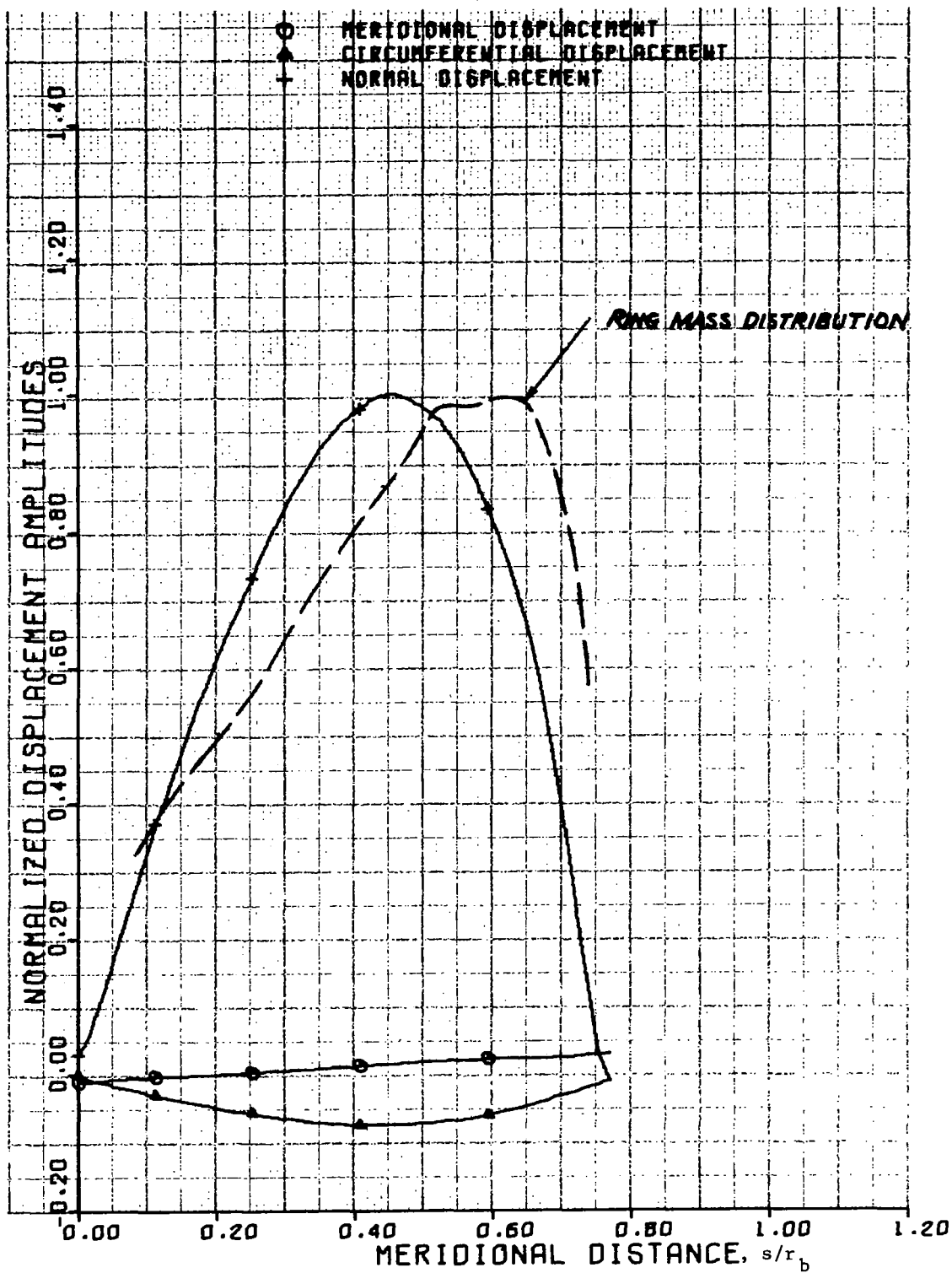


FIGURE 24. BUCKLING MODE DISPLACEMENTS
RING-STIFFENED CONE ($p/E = 1.86 \times 10^{-7}$, $r_b = 114$ IN.) $N = 6$

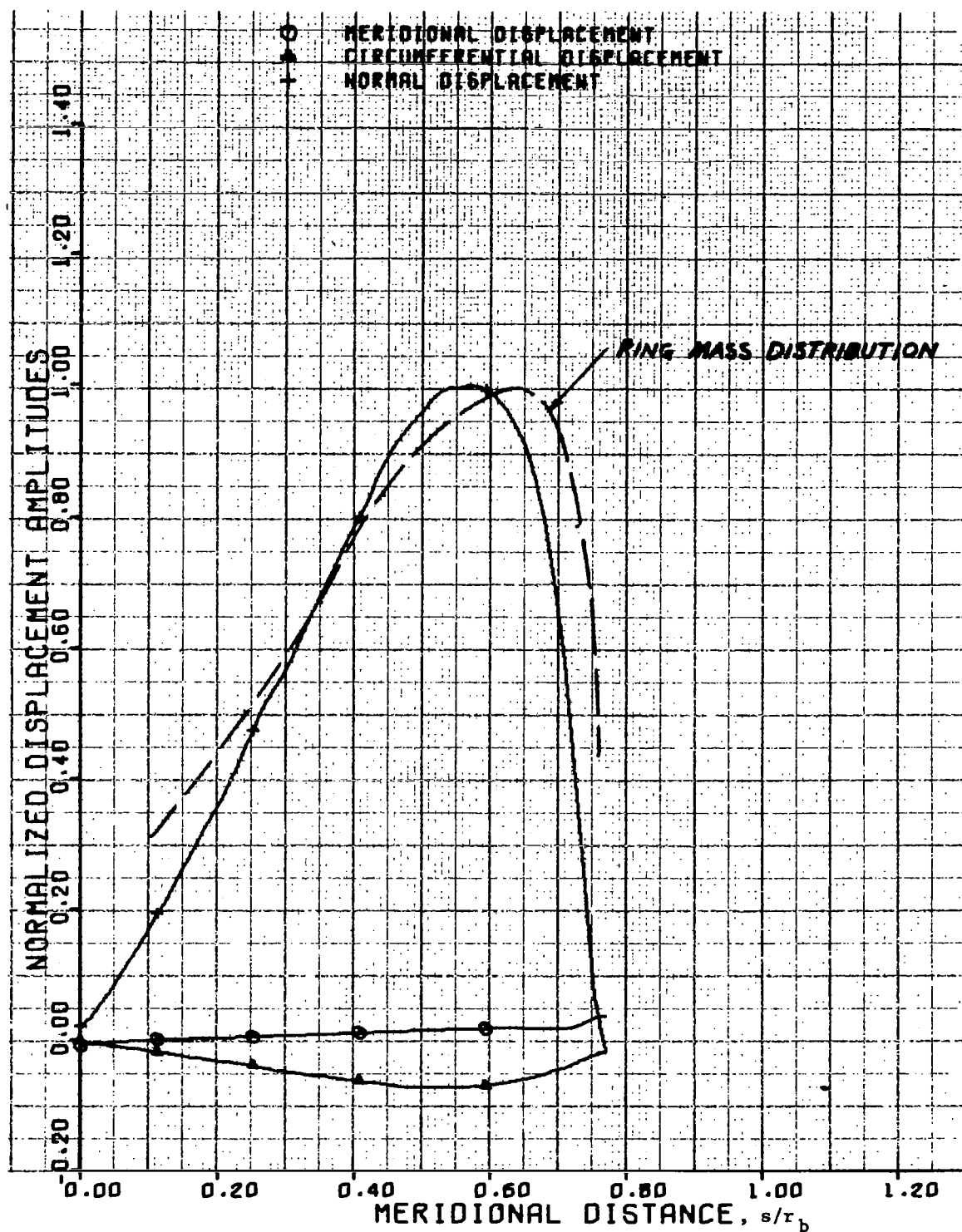


FIGURE 25. BUCKLING MODE DISPLACEMENTS
RING-STIFFENED CONE ($p/E = 9.28 \times 10^{-7}$, $r_b = 114$ IN.) $N = 5$

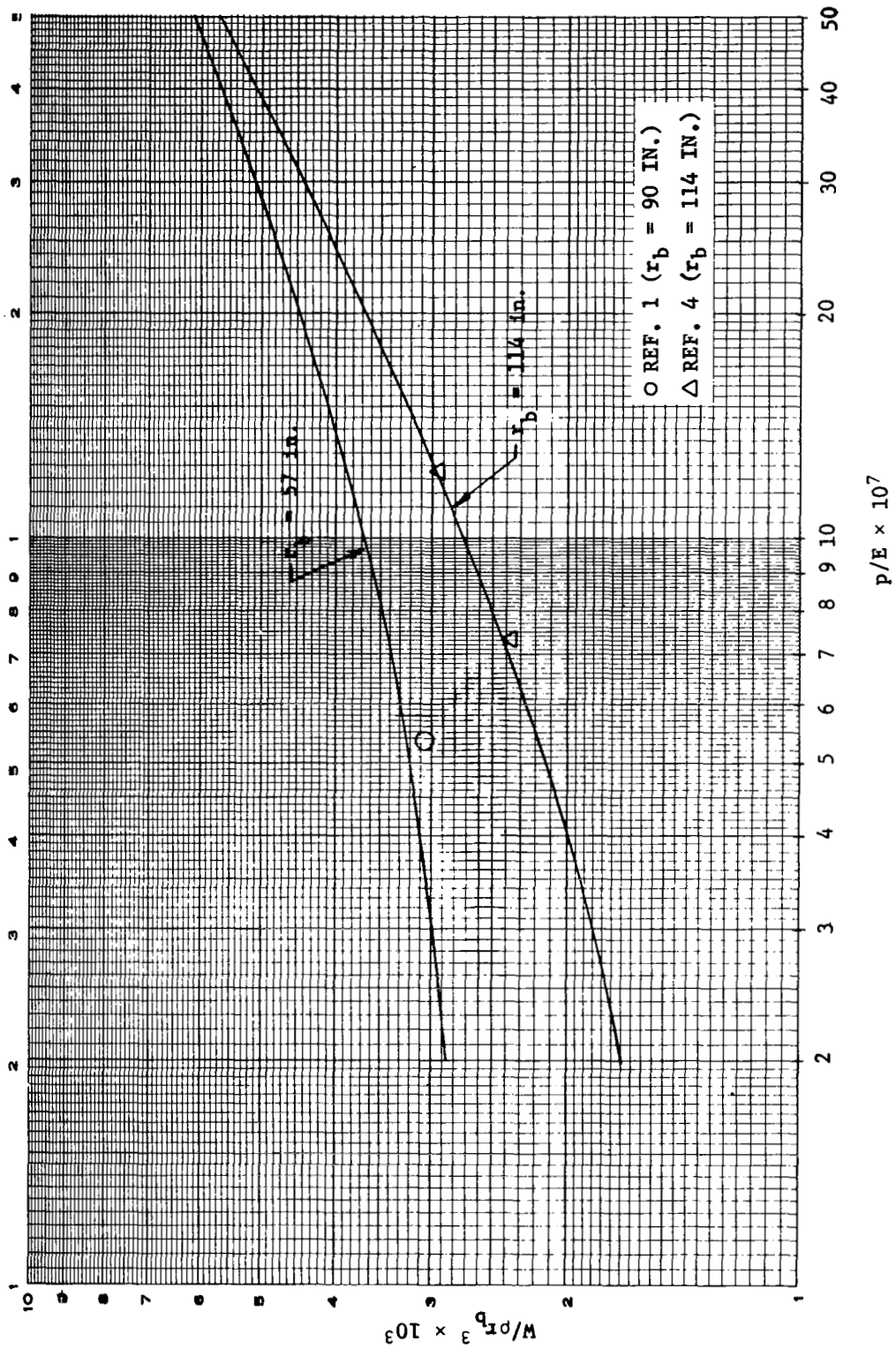


FIGURE 26. OPTIMIZED WEIGHT vs. BUCKLING PRESSURE
SANDWICH CONES (EXCLUDING ADHESIVE WEIGHT)

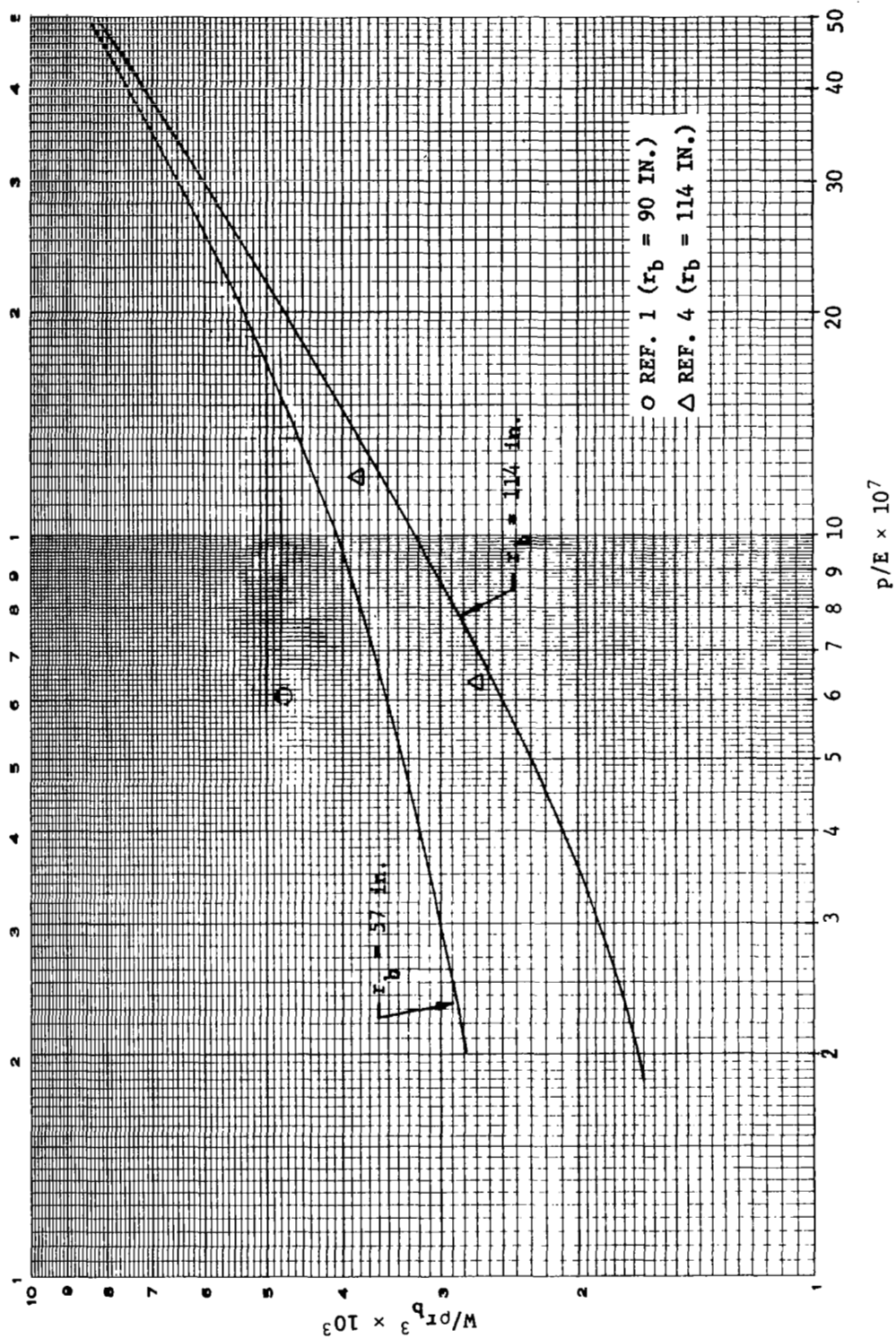


FIGURE 27. OPTIMIZED WEIGHT vs. BUCKLING PRESSURE
RING-STIFFENED CONES (INCLUDING RIVET WEIGHT)

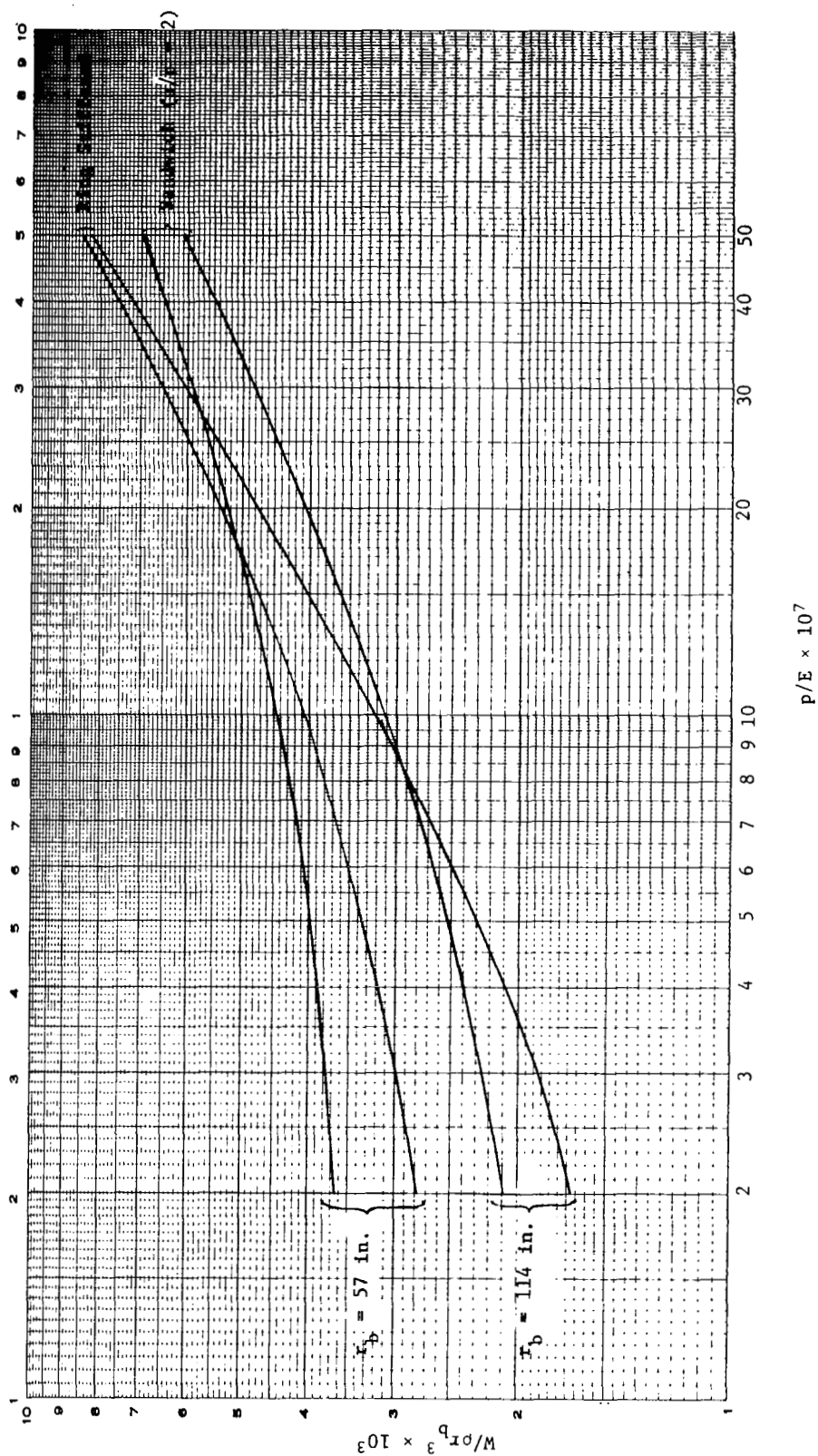


FIGURE 28. COMPARISON OF SANDWICH CONE WEIGHT (INCLUDING ADHESIVE)
WITH RING-STIFFENED CONE WEIGHT (INCLUDING RIVETS)